Mutation of a Cuticular Protein, *BmorCPR2*, Alters Larval Body Shape and Adaptability in Silkworm, *Bombyx mori*

Liang Qiao,*,†,1 Gao Xiong, *,1 Ri-xin Wang, *,1 Song-zhen He,* Jie Chen,* Xiao-ling Tong,* Hai Hu,* Chun-lin Li,* Ting-ting Gai,* Ya-qun Xin,* Xiao-fan Liu,* Bin Chen,† Zhong-huai Xiang,* Cheng Lu, *,2 and Fang-yin Dai*,2

*State Key Laboratory of Silkworm Genome Biology, Key Laboratory for Sericulture Functional Genomics and Biotechnology of Agricultural Ministry, Southwest University, Chongqing, 400715, China and †Institute of Entomology and Molecular Biology, College of Life Sciences, Chongqing Normal University, Chongqing, 401331, China

ABSTRACT Cuticular proteins (CPs) are crucial components of the insect cuticle. Although numerous genes encoding cuticular proteins have been identified in known insect genomes to date, their functions in maintaining insect body shape and adaptability remain largely unknown. In the current study, positional cloning led to the identification of a gene encoding an RR1-type cuticular protein, BmorCPR2, highly expressed in larval chitin-rich tissues and at the mulberry leaf-eating stages, which is responsible for the silkworm *stony* mutant. In the Dazao-*stony* strain, the *BmorCPR2* allele is a deletion mutation with significantly lower expression, compared to the wild-type Dazao strain. Dysfunctional BmorCPR2 in the *stony* mutant lost chitin binding ability, leading to reduced chitin content in larval cuticle, limitation of cuticle extension, abatement of cuticle tensile properties, and aberrant ratio between internodes and intersegmental folds. These variations induce a significant decrease in cuticle capacity to hold the growing internal organs in the larval development process, resulting in whole-body stiffness, tightness, and hardness, bulging intersegmental folds, and serious defects in larval adaptability. To our knowledge, this is the first study to report the corresponding phenotype of *stony* in insects caused by mutation of RR1-type cuticular protein. Our findings collectively shed light on the specific role of cuticular proteins in maintaining normal larval body shape and will aid in the development of pest control strategies for the management of *Lepidoptera*.

THE cuticle covering the entire body surface of insects not only participates in defense against pathogens and adverse environmental factors, but is also indispensable for constructing and maintaining external morphological characteristics and locomotion during the entire developmental process (Wigglesworth 1957; Delon and Payre 2004; Moussian *et al.* 2005). Therefore, the cuticle greatly enhances survival ability and adaptability of insects, ensuring its continued existence as one of the most successful life forms in the animal kingdom.

The cuticle is a complex composite material mainly comprising chitin fibers and proteins (Andersen *et al.* 1995; Moussian 2010). Chitin is the polymer of β-1,4-linked *N*-acetyl-D-glucosamine (Gilbert 2011, Chap. 7). In procuticles, chitin fibers are arranged in laminae in an antiparallel manner and superimpose each other, forming sheets of fibrils that are stacked in a helicoidal fashion, maintaining cuticle structure, elasticity, and stability (Bouligand 1965; Neville and Luke 1969; Moussian 2010). In terrestrial insects, the chitin content is positively correlated with body size, suggesting a close relationship with cuticle extension and expansion (Merzendorfer and Zimoch 2003; Lease and Wolf 2010).

Cuticular proteins (CPs), the principal structural constituents of cuticle, are encoded by more than 100 genes in known insect genomes (Andersen *et al.* 1995; Willis *et al.* 2005; Weinstock *et al.* 2006; Karouzou *et al.* 2007; Cornman *et al.* 2008; Futahashi

doi: 10.1534/genetics.113.158766
Manuscript received October 18, 2013; accepted for publication January 27, 2014; published Early Online February 10, 2014.
Supporting information is available online at http://www.genetics.org/lookup/suppl/doi:10.1534/genetics.113.158766/-/DC1.
Sequence data from this article have been deposited with the EMBL/GenBank Data Libraries under accession nos. KF672849.1 and KF672850.1.
[1]These authors contributed equally to this work.
[2]Corresponding authors: State Key Laboratory of Silkworm Genome Biology, Key Laboratory for Sericulture Functional Genomics and Biotechnology of Agricultural Ministry, Southwest University, No. 1 Tiansheng Rd., Beibei District, Chongqing, 400715, China. E-mail: fydai@swu.edu.cn; lucheng@swu.edu.cn

et al. 2008; Richards *et al.* 2008; Cornman and Willis 2009; Gilbert 2011, Chap. 5) and form a proteinaceous matrix in which chitin fibers are embedded (Neville 1975; Papandreou *et al.* 2010). CP–chitin interactions are necessary for the normal structure and physical properties of cuticle (Andersen *et al.* 1995; Rebers and Willis 2001; Karouzou *et al.* 2007; Cornman *et al.* 2008; Moussian 2010). Over half of the known cuticular proteins contain chitin-binding domains, including the Rebers & Riddiford (R&R) motif (two major groups, RR-1 and RR-2, and a minor form, RR-3), Tweedle motif, and chtDB2 domain (Rebers and Riddiford 1988; Magkrioti *et al.* 2004; Cornman *et al.* 2008; Jasrapuria *et al.* 2010; Tang *et al.* 2010; Willis 2010; Andersen 2011; Gilbert 2011, Chap. 5). Chitin-binding cuticular proteins are widely distributed at different development stages and play roles in the physical properties of the cuticle (Rebers and Riddiford 1988; Guan *et al.* 2006; Soares *et al.* 2007; Okamoto *et al.* 2008; Togawa *et al.* 2008; Charles 2010; Gilbert 2011, Chap. 5; Arakane *et al.* 2012; Jasrapuria *et al.* 2012). These proteins often have crucial biological functions, such as body-shape determination, cuticle integrity and mechanical properties maintenance, movement ability, and adaptability of the insect (Guan *et al.* 2006; Arakane *et al.* 2012; Jasrapuria *et al.* 2012).

The soft, flexible cuticle of *Lepidoptera* larvae not only bears pressure from the internal contents on the integument to stabilize the long cylindrical body, but is also conducive to movement and expanding feeding and survival areas (Carter and Locke 1993; Brackenbury 1997; Lin *et al.* 2009). However, the mechanisms by which cuticular proteins participate in body-shape stability and adaptability of *Lepidoptera* is presently unclear. Here, we focus on the silkworm as a *Lepidoptera* model to investigate the above issues. Positional cloning led to the identification of a gene encoding a RR1-type cuticular protein, BmorCPR2, responsible for the silkworm *stony* mutant. In the mutant, dysfunctional BmorCPR2 induces significantly decreased cuticle chitin content, abnormal distribution of internode and intersegmental fold, and marked reduction in tensile property of the cuticle. Accordingly, the conflict between growing body-cavity contents and opposing lower cuticle capacity gradually increases, leading to body hardness and tightness. The variant intersegmental fold also bulges out due to enhanced internal pressure, resulting in a malformed body shape. Additionally, the hard body and bulges seriously affect the adaptability of the mutant, such as crooking and shock-buffering abilities. Therefore, characterization of this gene and its underlying effects may contribute to our understanding of the role of cuticular proteins in maintaining of external morphological characteristics of *Lepidoptera* larvae and control of *Lepidoptera* pests.

Materials and Methods

Silkworm strains

The wild-type strains—Dazao, 05-111, 06-072, 20-230, Xiafang, 01-070, 16-060, 05-050, 16-100, 16-105, C108, 06-920, 04-702—and *stony* mutant strains—Dazao-*stony* (near isogenic line of Dazao) and 12-220 (donor parent of *stony* locus)—used in this research were obtained from the silkworm gene bank in Southwest University. The near isogenic lines have been backcrossed with Dazao over 24 generations; other wild-type and *stony* mutant strains inbred at least 20 generations. Silkworms were reared on fresh mulberry leaves under a 12 hr/12 hr light/dark photoperiod at 24°.

Phenotype analysis, physiology test, and behavior assays

The phenotypes of Dazao and Dazao-*stony* individuals and excrement appearance were recorded using a digital camera (Canon EOS 5D Mark III). The cuticle was dissected, and adhesive tissues were scraped off and cleaned with ddH_2O. Internode, anterior, and posterior parts of internode, intersegmental fold of treated cuticle were divided and measured using a stereo microscope (Nikon SMZ1500), digital camera, Adobe Photoshop CS3, and image J software. Based on the principle of buoyancy, we surveyed the exact larval body volume in a volumetric cylinder. Additionally, midgut contents from these individuals were dislodged, lightly cleaned with ddH_2O, and torrified at 60°. The ratio of midgut contents mass to individual volumes analyzed. For the physiology tests (dropping experiment; the flexibility and nesting ability of segments) and behavior assays, detailed operation are listed in Supporting Information, File S1.

Positional cloning

Mapping of *stony* locus and bioinformatic analysis of candidate regions were performed, as described previously (Dai *et al.* 2010). In Bm_nscaf2827 (chromosome 8), we identified polymorphic PCR markers between the parents, Dazao-*stony* and C108, and assessed these in BC_1F individuals. In BC_1M progeny, individuals exhibiting *stony* phenotype (homozygosis on *stony* locus) were genotyped. The primers used for mapping are listed in Table S1.

DNA sequence cloning

Total RNAs were extracted from the integuments of wild type (Dazao and other WT strains) and *stony* mutant (Dazao-*stony* and *stony* parent strain, 12-220) on day 4 of the fifth-instar larvae using TRIzol (Invitrogen), according to the manufacturer's instructions. The 5′-UTR and 3′-UTR of *BmorCPR2* and *BmorCPR3* were amplified using the GeneRacer Kit (Invitrogen). We additionally amplified the genome sequence ~2.78 and ~0.83 kb upstream of *BmorCPR2*. PCR products were cloned into the pMD19-T vector for sequencing. The primers used for cloning are listed in Table S1.

Expression profile of BmorCPR2

Semiquantitative RT–PCR was performed as described previously (Dai *et al.* 2010). The development stages include hatching to moth stage. Tissues of Dazao examined on day 4 of the fifth-instar larvae included head, integument, trachea, malpighian tubes, midgut, gonads, fat body, anterior/middle/posterior

silk gland, nerves, muscle, and hemocyte. Primers designed for RT–PCR are shown in Table S1. The BmActin3 gene was used as an internal control.

20-Hydroxyecdysone (20E) treatment

Day 4 of the fifth-instar larvae (wild type) were treated with 20E (dissolved in 10% ethanol, injected with 3 μg per individual) or 10% ethanol (control), and *BmorCPR2* expression detected at 3 and 24 hr after injection.

Quantitative RT–PCR

Quantitative RT–PCR was performed as described previously (Dai *et al.* 2010), using the StepOneTM real-time PCR xystem (ABI). Primers used for qRT–PCR are listed in Table S1.

Quantification of chitin content

The larval segment cuticle of Dazao, Dazao-*stony*, internode, and the intersegmental fold of Dazao and Dazao-*stony* larvae, anterior and the posterior parts of the internode of Dazao, and posterior parts plus intersegmental fold of Dazao were dissected. After eliminating adherent tissue completely and cleaning with ddH_2O, materials were dried under 60° and weighed with an analytical balance (METTLER-MS105DU). Extraction and determination of chitin were performed according to the protocol of Kunyan Zhu (Zhang and Zhu 2006) with slight modifications. All determinations were performed on three or four biological replicates for each sample.

SDS–PAGE and chitin binding

The cuticles of day 5 of the fifth-instar Dazao and Dazao-*stony* larvae were dissected, and adherent tissue were removed and cleaned with nuclease-free and protease-free water. Total proteins were extracted according to the method of Tang *et al.* (2010) and detected using 15% SDS–PAGE. For the chitin binding experiment, detailed operations are listed in File S1.

Liquid chromatography tandem mass spectrometry analysis

Selected gel bands were excised and subjected to liquid chromatography tandem mass spectrometry (LC–MS/MS) analysis (LTQ VELOS, Thermo Finnigan, San Jose, CA). Detailed operation are listed in File S1.

RNA interference

ds*BmorCPR2* and ds*Red* were synthetized using the RiboMAX large-scale RNA production system-T7 (Promega) based on the PCR templates according to the manufacturer's instructions. The injection time selected according to the *BmorCPR2* expression pattern was the eating-less period of fourth instar (day 3 of the fourth instar to the period of molting). dsRNA was diluted to 10 μg/μl, and a dose of 110 μg was administered to each individual. Larvae at 16 hr of fourth molting and beginning of fifth instar were used to detect *BmorCPR2* and *BmLcp22* expression. Individuals from the ds*BmorCPR2* group at the beginning of the fifth instar were employed for counting interference efficiency. Meanwhile, chitin contents of the interference and control groups were determined. Primers for PCR are listed in Table S1.

Tensile property of larval cuticles

The cuticles of day 5 of the fifth instar Dazao and Dazao-*stony* larvae were dissected and adherent tissue was removed, followed by cleaning with ddH_2O. The cuticle was spread smooth and trimmed into a rectangle. Tensile properties were determined in the longitudinal direction (head to tail), whereby the length of the rectangular pattern was from semilunar to star marking, and the width was taken as the distance between both sides of the spiracle on the dorsal side (spread smooth). Tensile properties in the transversal direction were determined as follows: the length of the rectangular pattern represents the distance between both sides of the spiracle on the dorsal side (spread smooth), while the width is from the start of the third abdominal segment to the end of the fourth abdominal segment. The sample was incubated for 30 min at room temperature and 80% relative humidity and was rapidly fixed between two grips of the DMA Q800 Dynamic Mechanical analyzer. Samples were stretched according to the strain–stress mode (at ambient temperature, stress varied linearly at a constant rate) to test their mechanical properties. All determinations were performed on three biological replicates for each sample.

Results and Discussion

Stony mutant larva displays altered morphologic characteristics with deficiency in adaptability

The peculiar body shape of *stony* is mostly evident in the post margins of every larval segment as distinct bulges, and the mutant is more slender with a smaller body size (Figure 1A). Dissection of *stony* mutant larvae revealed a higher ratio of midgut content mass to body volume, compared to wild type (Figure 1D). However, the ratio of internodes containing internal contents in every segment was significantly lower than that of wild type (Figure 1, B and C). Furthermore, the tails of the fifth-instar larvae usually cocked up when satiated with mulberry leaf (Figure S1A). The rectocele appeared easily upon defecation, and smaller amounts of excrement were produced (Figure S1, B and C). These phenotypic and physiological characteristics suggest stronger pressure in the body of *stony* mutant corresponding to hardness and tightness to touch. In the dropping experiment, 90% *stony* individuals (with smaller gravitational potential energy, GPE) breached the cuticle, accompanied by outflow of internal tissues and hemolymph, while only one wild-type individual displayed similar symptoms (Figure 1E, Figure S1, D and E, File S1, and File S2). The data indicate that the stiff, tight body of *stony* significantly lowers its ability to buffer shock. Air injection showed nestification (the somite shortening, namely, the anterior part of the latter segment shrinks to the posterior part of the former one) between every two conjoint segments of wild type, leading

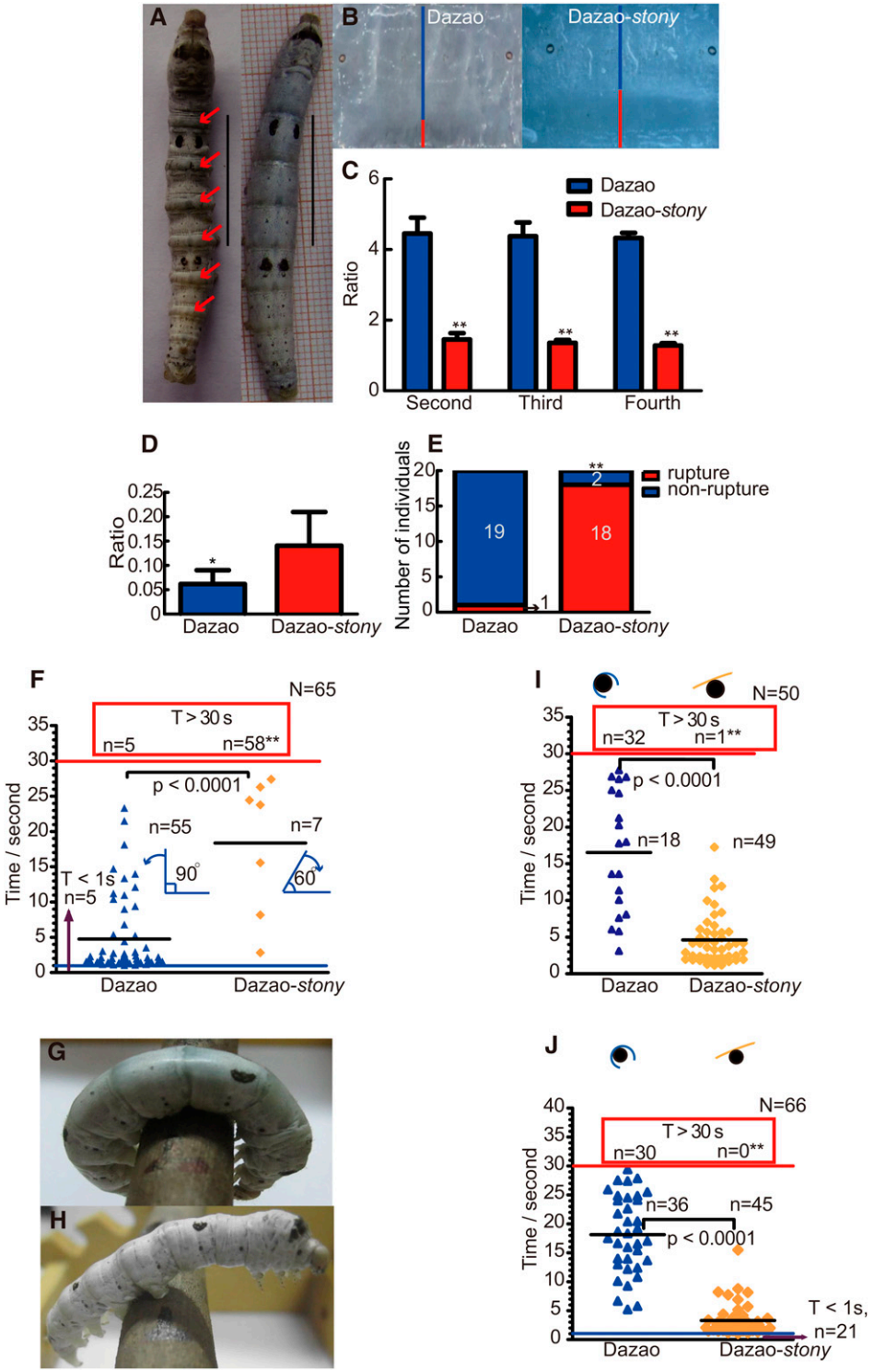

Figure 1 Characterization of Dazao-*stony* mutant. (A) Phenotype of the dorsal side of Dazao (right) and Dazao-*stony* (left). Red arrows indicate bulges. Scale bar, 2 cm. (B) Dorsal cuticle anatomy characteristics of Dazao and Dazao-*stony*. The blue and red lines represent the length spanned by internode and intersegmental fold, respectively. (C) Ratios between the length of internode and intersegmental fold in the second, third, and fourth abdomen segments of Dazao and Dazao-*stony*, respectively (n = 5). (D) Ratio of the midgut content mass and larval volume between Dazao and Dazao-*stony* (n = 6). Data represent mean values ±SD. Student's t-test; *, $P < 0.05$; **, $P < 0.01$ (C and D). (E) Statistics of breached Dazao and Dazao-*stony* larvae in dropping experiment. (χ^2-test; **, $P < 0.01$.). (F) Analysis of the larval abdominal crooking test. Both red and blue lines represent threshold time. The numbers in the red box indicate individuals that cannot crook to abdomen in 30 sec. (χ^2-test; **, $P < 0.01$). The counterclockwise and clockwise arrowheads represent the crooking angles in Dazao and Dazao-*stony*, respectively. Both black lines represent the average time of abdomen bending between Dazao and Dazao-*stony* within the threshold time. (Mann–Whitney U-test, $P < 0.0001$). (G and H) Phenotypes of grasping mallet of Dazao and Dazao-*stony*, respectively. (I and J) Analysis of grasping tests on the large and small diameter mallets of Dazao and Dazao-*stony*, respectively. Both the red and blue lines signify threshold time. The numbers in the red box represent individuals that grasp for >30 sec. (χ^2-test; **, $P < 0.01$). Both black lines represent the average time of grasping between Dazao and Dazao-*stony* within the threshold time (Mann–Whitney U-test, $P < 0.0001$). The black solid circle represents the cross-section of the mallet. Blue and yellow curves represent the ventral bending of Dazao and Dazao-*stony*, respectively.

to shorter larvae (Figure S1, F and G). However, nesting was not observed for the *stony* mutant owing to the bulges produced by intersegmental fold of its abdominal segment, signifying deficiency in flexibility (Figure S1, H and I).

Based on these results and known kinematic characteristics of caterpillars (Brackenbury 1997; Lin *et al.* 2009), we designed a series of behavioral experiments to test the athletic ability of *stony* mutant. The abdominal crooking test revealed that >90% wild-type individuals easily crook to abdomen within 30 sec, with a crooking angle of >90°; however, ~89% *stony* individuals were unable to perform crooking within 30 sec, even over prolonged times, and the remaining *stony* individuals with crooking ability performed the activity over a longer time and could not crook to >60°, and the *stony* mutants displayed a severe reverse angle bending in the crooking test (Figure 1F, Figure S1, H and

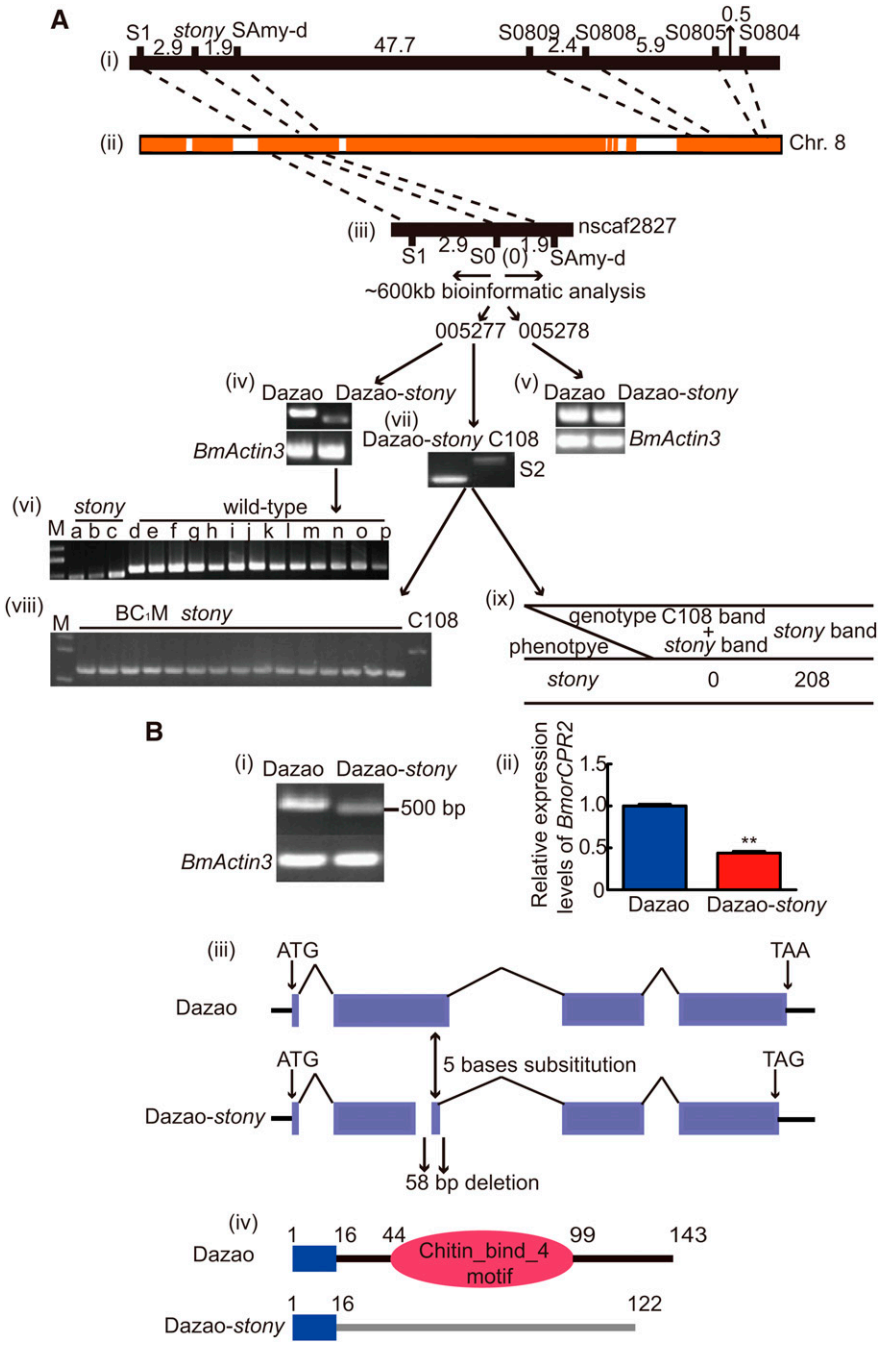

Figure 2 Genetic basis of the *stony* mutant. (A) Positional cloning of *stony* locus. (i) Preliminary mapping of *stony* locus. (ii) Location of markers on the physical map of chromosome 8. The yellow and white regions represent scaffolds and gaps, respectively. (iii) Fine mapping of *stony* locus. (iv v) Transcript analysis of *BGIBMGA005277* and *BGIBMGA005278* in Dazao and Dazao-*stony*, respectively. (vi) Transcript analysis of *BGIBMGA005277* among different *stony* and wild-type strains (a–c) *stony* mutant strains; (a and b) Dazao-*stony*; (c) 12-220; (d–p) wild-type strains (Dazao, 05-111, 06-072, 20-230, Xiafang, 01-070, 16-060, 05-050, 16-100, 16-105, C108, 06-920, 04-702)). (vii) The polymorphism marker S2. (viii–ix) Genotyping analysis between S2 and *stony* locus. (B) Scheme of *BmorCPR2* transcripts of Dazao and Dazao-*stony*. (i) Full-length *BmorCPR2* cDNA in Dazao and Dazao-*stony*. (ii) Relative expression of *BmorCPR2* between Dazao and Dazao-*stony* in larval cuticles (mean values ±SD; Student's *t*-test; **, $P < 0.01$, $n = 3$). (iii) Transcripts of *BmorCPR2* from Dazao and Dazao-*stony*. (iv) Domain organization of BmorCPR2 in Dazao and Dazao-*stony*.

I, and File S3). Since the crooking ability of the abdomen is weak, irrespective of mallet diameter, it is difficult for the *stony* mutant to grasp, and almost all individuals dropped from the mallet within 30 sec due to loss of balance (Figure 1, G–J, File S4, and File S5). Moreover, within the threshold time (30 sec), the average grasping time of dropped *stony* individuals was significantly shorter than that of wild type (Figure 1, I and J, File S4, and File S5). Subsequent inversion and food inducement tests showed degeneration of turning over and crawling abilities in the mutant (Figure S1, J, and K, File S6, File S7, and File S8). In view of the abnormal body shape and adaptability deficiency, we speculate that the gene responsible for the mutant phenotype is associated with cuticle abnormality.

The stony locus encodes BmorCPR2

We mapped the *stony* locus within a ~1.5-Mb region on Bm_nscaf2827 using 208 BC_1 individuals (*stony* phenotype) (Figure 2A-i and Figure 2A-ii). Subsequently, we designated the polymorphism marker, S0, at the ~1544-kb position on Bm_nscaf2827 (reference as 1 cM ~ 300 kb in silkworm (Yamamoto *et al.* 2008) and the genetic distance between *stony* and SAmy-d in the linkage map). Further linkage analysis showed that the S0 marker is tightly linked with the

stony locus (Figure 2A-iii). We analyzed the upstream and downstream sequences of S0 in the silkworm database. Close to the S0 marker, we observed two predicted gene models encoding RR1-type chitin-binding cuticular proteins that play an important role in construction of the soft insect cuticle (Andersen *et al.* 1995, 2011; Togawa *et al.* 2008; Moussian 2010; Willis 2010) (Figure 2A-iii). Full-length cDNA of *BGIBMGA005278* (*BmorCPR3*) was not different in wild type and *stony*, and the gene expression patterns were relatively similar (Figure 2A-v, and Figure S2). However, cDNA of *BGIBMGA005277*, previously designated *BmorCPR2* or *Larval cuticular protein 17* (Nakato *et al.* 1997; Futahashi *et al.* 2008), had an obvious deletion, and its expression was significantly reduced in Dazao-*stony* (Figure 2A-iv). The amplified *BGIBMGA005277* cDNA fragment was assessed in two *stony* (Dazao-*stony*, 12-220) and 13 wild-type strains (Dazao, 05-111, 06-072, 20-230, Xiafang, 01-070, 16-060,119 05-050, 16-100, 16-105, C108, 06-920, 04-702) with different genetic backgrounds. The results indicate that deletion occurs specifically in the *stony* mutants (Figure 2A-vi). Simultaneously, we designed the polymorphism marker, S2, according to the genome sequence of *BmorCPR2* (Figure 2A-vii). Genotyping of the marker revealed no recombination between S2 and the *stony* locus (Figure 2, A-viii and -ix). Accordingly, we conclude that *BmorCPR2* is a candidate gene responsible for the *stony* mutant. Full-length *BmorCPR2* cDNA (accession no. KF672849.1) is 547 bp encoding 143 amino acids residues and contains a typical chitin-binding domain (Figure 2B-i, d, and Figure S3). Orthologs of this gene are widely distributed in different *Lepidopterous* insects (identities range from 40 to 75%), indicative of conservation (Figure S3B, and Table S4). However, the *BmorCPR2* transcript contains a 58-bp deletion and 5-bp single-nucleotide substitution in the second exon in Dazao-*stony*, resulting in a frameshift and premature stop codon (Figure 2, B-iii and C, and Figure S3A). In the aberrant transcript (accession no. KF672850.1), the entire chitin-binding domain was lost (Figure 2B-iv and Figure S3A). In addition, deletion of BM2A-like transposon located ~2.78 kb upstream and insertion of Ins11-like transposon ~0.83 kb upstream of *BmorCPR2*, combining the premature termination codon, led to significantly reduced levels of *BmorCPR2* in Dazao-*stony* (Figure 2B-ii and Figure S4) (Chang *et al.* 2007; Feschotte 2008).

High expression of the *BmorCPR2* gene during the interval of larval molting is negatively correlated with the titer of 20E, indicating that the expression pattern of *BmorCPR2* is synchronized with the procuticle (the chitinous cuticle) development during larval stages (Mizoguchi *et al.* 2001; Kiguchi 1981) (Figure 3, A, B, C, E, and F). Additionally, expression of *BmorCPR2* was reduced from the wandering stage to the early stage of pupation, and in sequential development stages, *BmorCPR2* expression was reduced significantly or to nearly undetectable levels (Figure 3C). These findings coincide with the visible obvious phenotype in the molting interval of *stony* larvae. In chitin-rich tissues, such as head, integument, and trachea (Gilbert 2011, Chap. 5), *BmorCPR2* was also highly expressed, in keeping with the chitin-binding domain (Figure 3D). However, the reason underlying high expression of *BmorCPR2* in fat body remains unclear (Figure 3D).

BmorCPR2 affects cuticle chitin content and larval molting via effects on chitin binding

Total proteins extracted from larval cuticle of Dazao and Dazao-*stony* showed that the mutant protein is devoid of a band at ~15.3 kDa, compared with wild-type Dazao (Figure 4A and Table S2). Mass spectrometry findings confirmed that this band represents BmorCPR2 protein (a major component), which is absent at the corresponding position in the gel in *stony*, indicative of defective BmorCPR2 protein in the mutant (Figure 4A, C; Table S2). Chitin binding assay of total proteins extracted from the wild-type cuticle revealed ~15.3-kDa protein bands in chitin bead deposits, signifying binding of these proteins to chitin (Figure 4B). Meanwhile, mass spectrometry results revealed that the electrophoretic bands contain BmorCPR2, validating the capacity of BmorCPR2 to bind chitin (Figure 4, B and C, and Table S2). These findings are consistent with the structural characteristics of the protein and results of Tang *et al.* (Rebers and Riddiford 1988; Futahashi *et al.* 2008; Tang *et al.* 2010; Willis 2010; Andersen 2011). Subsequently, we assayed the chitin content of Dazao and Dazao-*stony* larval cuticles (day 5 of the fifth instar). Notably, the cuticle chitin content in Dazao was ~1.76 times that in Dazao-*stony* (Figure 4D). Naked chitin fibers need to interact with chitin-binding protein to stabilize the helicoidal layers of cuticle (Rebers and Riddiford 1988; Rebers and Willis 2001; Merzendorfer and Zimoch 2003; Moussian 2010). The largest member of these chitin-binding proteins is the CPR family, which may contribute to coordinating the interactions between chitin and the proteinaceous matrix (Rebers and Riddiford 1988; Rebers and Willis 2001; Togawa *et al.* 2004; Magkrioti *et al.* 2004; Tang *et al.* 2010; Willis 2010; Andersen 2011), and RR-type chitin-binding protein, chitin, and chitinase are colocalized in the procuticle (Moussian *et al.* 2006; Chaudhari *et al.* 2011, 2013; Arakane *et al.* 2012). The recent study on *Tribolium castaneum* indicated that the TcCPR4 (a RR1-type cuticular protein) distribute the region nearby chitin laminae and can affect the chitin content (Arakane 2013). Based on these results, we hypothesized that BmorCPR2 plays an important role in maintaining chitin content of the cuticle. However, it remains to be established whether BmorCPR2 protects chitin through combining and packaging chitin fibers, similar to the chitin-binding protein, knickkopf (Moussian *et al.* 2006; Chaudhari *et al.* 2011). RNAi experiments were performed to specifically reduce the expression levels of *BmorCPR2* (Figure 4F and Figure S5, A and B). Our results revealed that 42% of the individuals in the ds*BmorCPR2* group display molting difficulties at the beginning of the fifth-instar larvae (*dsRed* as a control) (Figure 4E; Table S3). Moreover, this phenotype occurred

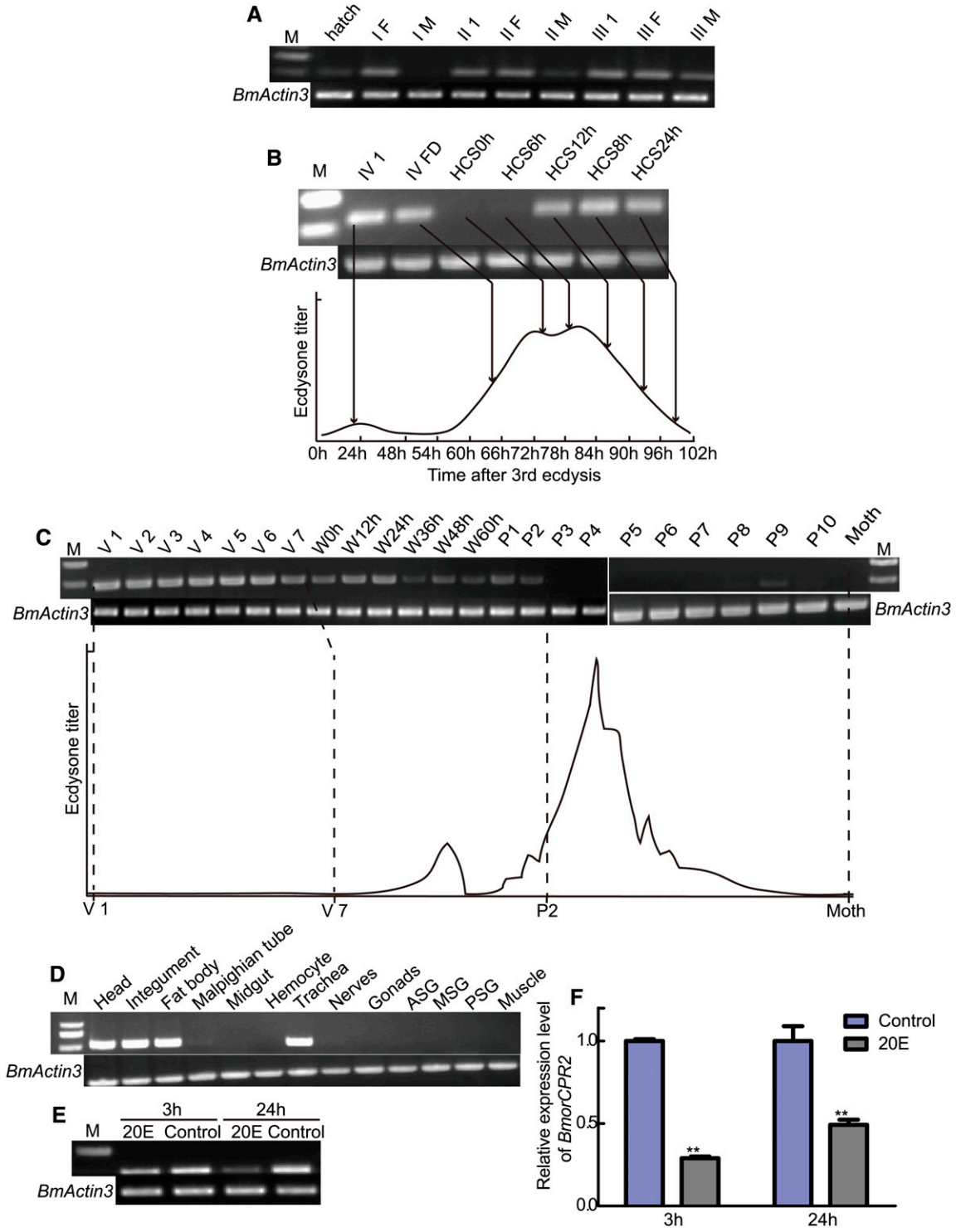

Figure 3 Expression profiles of *BmorCPR2* in Dazao. *BmActin3* was used as the internal control for RT–PCR. (A–C) Temporal expression profiles of *BmorCPR2* from the hatch to moth stage. I–II, larvae from first to third instar. (F) Feeding stage. M, molting stage. IV 1, day 1 of the fourth-instar larvae (20 hr after third ecdysis). FD, feeding activity decline stage (about 64 hr after third ecdysis), HCS0-24h, hours after head capsule slippage (about 75–99 hr after third ecdysis). V 1–V 7, days 1–7 of the fifth-instar larvae. W0h–W60h, 0–60 hr of the wandering stage; P1–P10, days 1 to 10 of pupation. The developmental changes in hemolymph ecdysteroid titer are based on the data as previously described (Mizoguchi *et al.* 2001; Kiguchi 1981). (D) Spatial expression of *BmorCPR2* on day 4 of the fifth-instar larvae in Dazao. ASG, MSG, and PSG: anterior, middle, and posterior silk gland, respectively. (E and F) Expression patterns of *BmorCPR2* after 20E treatment. Data are presented as mean values ±SD. Student's *t*-test, **, $P < 0.01$, $n = 3$.

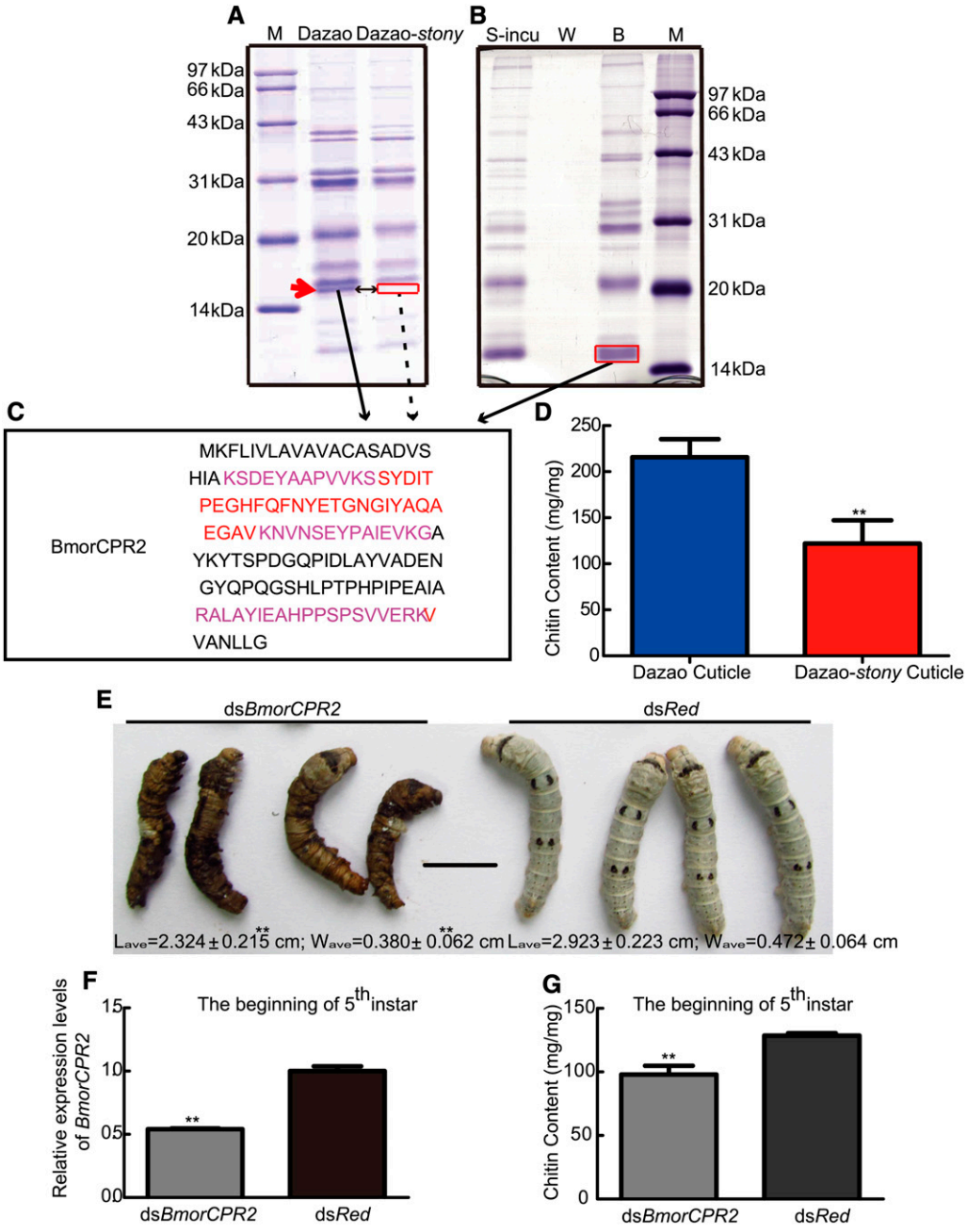

Figure 4 Biochemical function of BmorCPR2. (A) SDS–PAGE profiles of larval cuticle total proteins extracted from Dazao and Dazao-*stony*. The red arrow represents BmorCPR2, which was absent in Dazao-*stony*. M, molecular mass markers; type, midrange protein molecular weight markers (Shanghai Generay Biotech). (B) Chitin-binding assay with cuticle total proteins of Dazao. S-incu, supernatant removed via centrifuging after incubation. W, second collected eluent after centrifugation. B, liquid obtained from centrifuged chitin resin treated with denaturant. Red boxes indicate the gels used for LC–MS/MS analysis. Solid arrows represent BmorCPR2 detected using LC–MS/MS; dotted arrows indicate BmorCPR2 that is not detectable with LC–MS/MS. M, molecular mass markers; type, midrange protein molecular weight markers (Shanghai Generay Biotech). (C) Corresponding LC–MS/MS peptides of the identified protein (BmorCPR2) in cuticle proteins (red and purple) and chitin binding assay (purple). (D) Comparison of the cuticle chitin contents between Dazao and Dazao-*stony*. (n = 4). (E) Phenotypes of larvae at the beginning of fifth instar subjected to RNAi. Scale bar, 1 cm. L_{ave} and W_{ave}, the average length and width (the third abdomen segment), respectively, of larvae. (n = 10). (F) Relative expression levels of *BmorCPR2* at the beginning of fifth-instar larvae subjected to RNAi (n = 3; *dsRed* as a control). (G) Comparison of the cuticle chitin content at the beginning of fifth-instar larvae between ds*BmorCPR2* and control groups (n = 4; *dsRed* as a control). Data represent means ±SD. Student's *t*-test, ** $P < 0.01$ (D–G).

more frequently in the *stony* mutant, compared with wild type (Figure S1L). Individuals injected with ds*BmorCPR2* that displayed molting difficulty were hard to touch, had smaller body size, and became dark owing to effusion of blood (these individuals were still alive) (Figure 4E). After peeling the old cuticle of individuals in the abnormal interference group, we observed that internal organs break new cuticles and overflow (data not shown). The chitin content in the new cuticle of ds*BmorCPR2* individuals (with RNAi phenotype) was significantly lower than that of the control group (*dsRed* as a control) (Figure 4G). The process of cuticle extension and increasing of body size require chitin as crude material (Merzendorfer and Zimoch 2003; Lease and Wolf 2010), and therefore simultaneously, larval molting is a critical period for the formation and growth of new cuticles. Accordingly, we propose that suppression of *BmorCPR2* decreases the chitin content and level of *BmorCPR2*, resulting in limitation of remodeling and extension of the larval cuticle and weakened body cavity capacity. Increasing internal pressure makes the body tight and hard

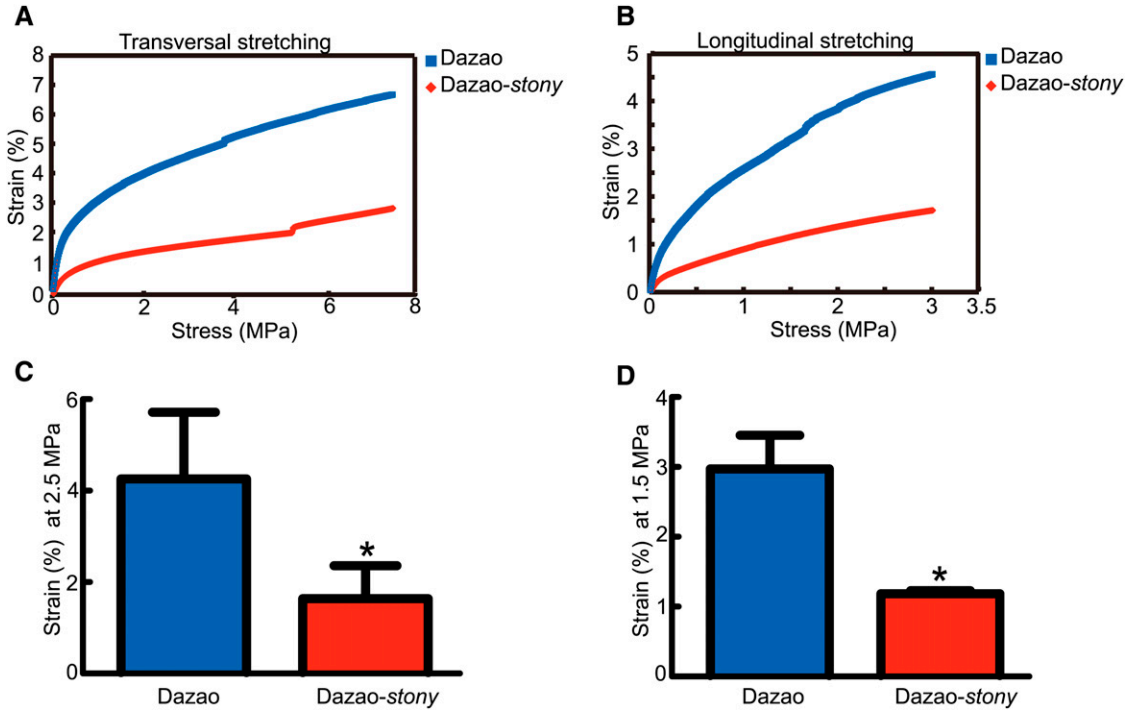

Figure 5 Effects of BmorCPR2 on mechanical properties of larval cuticle. (A) Relationship between stress and strain with transversal stretching. (B) Relationship between stress and strain with longitudinal stretching. (C) Dazao and Dazao-*stony* cuticles at transversal stress of 2.5 MPa. (D) Dazao and Dazao-*stony* cuticles at longitudinal stress of 1.5 MPa. Data represent mean values ±SD. Student's *t*-test, *, $P < 0.05$, $n = 3$ (C–D).

to touch (Carter and Locke 1993; Merzendorfer and Zimoch 2003). In this case, when the larvae molt, abdominal contraction and powerful pressure within the body lead to elongation-limited cuticle rupture, bleeding, and organ overflow. Based on these results, we conclude that the *BmorCPR2* gene plays important roles in the maintenance of chitin content of larval cuticle as well as extension of new cuticles and increase of body size during the molting stage.

BmorCPR2 is involved in maintaining the tensile property of the larval cuticle

The insect cuticle requires elongation and tensile properties to accommodate the increasing body cavity content during growth and development (Wigglesworth 1957; Locke 1970; Richards and Davies 1977; Moussian 2010). The tensile property of the cuticle in Dazao and Dazao-*stony* larvae were examined (Figure S6). Compared to Dazao, Dazao-*stony* needed more stress under the same strain conditions in the longitudinal and transversal (Figure 5, A and B). Within the strictly linear relationship between stress and strain, when longitudinal tensile stress was 1.5 MPa, the strain of Dazao-*stony* was only one-third that of wild type, and at 2.5-MPa transverse stretch stress, strain of the mutant was also far lower than that of wild type (Figure 5, C and D). In insects, chitin content and chitin–cuticular protein interactions are essential for maintaining the normal mechanical properties of the cuticle. In Dazao-*stony*, dysfunctional BmorCPR2 affects the chitin content as well as interactions between chitin and BmorCPR2, in turn, significantly attenuating the tensile properties of the cuticle and further decreasing body cavity capacity. This was similar to the phenotype characteristics of *Manduca sexta* when reducing larval cuticle tensile property (via treatment with cyromazine) (Reynolds and Blakey 1989; Kotze and Reynolds 1990). Under these situations, greater pressure in the body cavity caused by reduced cuticle tensile properties may be another vital factor for the hard body and defective athletic ability of the *stony* mutant.

Dysfunction of BmorCPR2 may cause the appearance of posterior internode similar to intersegmental fold in stony mutant

To determine the reasons underlying the abnormal ratio between internode and intersegmental folds in *stony*, we investigated the expression patterns of the related cuticular proteins and chitin content in different parts of the dorsal segment cuticle in detail. The internode of Dazao is further divided into anterior part (AP) and posterior part (PP) (Figure 6A-i, -ii, -iii). *BmorCPR2* displayed similar expression patterns to *BmLcp18*, *BmLcp22*, and *BmLcp30*, three known larval RR1-type chitin-binding cuticular protein genes (Nakato *et al.* 1997; Togawa *et al.* 2004), in different regions of Dazao larval cuticle. All genes were expressed more highly in internodes than in intersegmental folds. They also had higher expression in PP, specifically, in the posterior part of the segment (including PP and intersegmental fold) than in AP (Figure 6A-iv and Figure S7A-i, -ii, -iii). Analogous patterns were additionally obtained with regard to

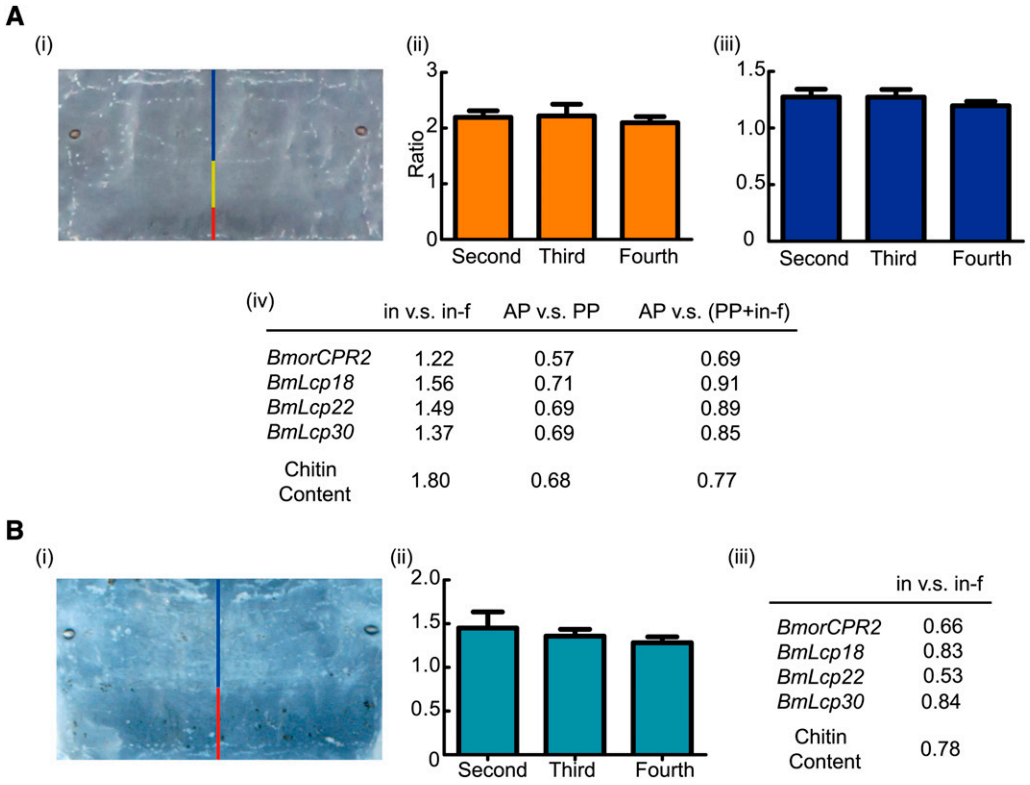

Figure 6 Gene expression profiles and chitin distribution in various parts of segmental cuticle in Dazao and Dazao-*stony*. (A) Cuticular gene expression profiles and chitin distribution in different parts of Dazao dorsal segment cuticle. (i) Images of various parts of the dorsal segment cuticle in Dazao. Blue, yellow, and red lines represent the AP and PP of the internode (in), and the intersegmental fold (in-f), respectively. (ii) Ratio of the AP and PP lengths in the second, third, and fourth abdomen segments of Dazao (n = 5). (iii)Ratio of AP length and remaining parts in the second, third, and fourth abdomen segments of Dazao (n = 5). (iv)Ratios of genes expression levels and chitin content in different parts of Dazao dorsal segment cuticle. (B) Cuticular gene expression profiles and chitin distribution in different parts of Dazao-*stony* segment. (i) Images of various parts of the dorsal segment cuticle in Dazao-*stony*. The blue and red lines represent the internode (in) and intersegmental fold (in-f), respectively. (ii) Ratio of the internode and intersegmental fold lengths in the second, third, and fourth abdomen segments of Dazao-*stony* (n = 5). (iii) ratios of genes expression levels and chitin content in different parts of Dazao dorsal segment cuticle. Further details can be found in the Figure S7.

chitin content in these regions (Figure 6A-iv and Figure S7A-iv, -v, -vi). Compared to the intersegmental fold, higher gene expression and chitin levels are required in the internode to fit growth (expanded circle area) and satisfy the increasing demand to hold body-cavity contents. In particular, the higher gene expression and chitin content in PP than in AP corresponded well with its enhanced flexibility and tensile property. Among the four cuticle genes examined, only *BmorCPR2* displayed sequence differences between Dazao and Dazao-*stony* (Figure 2, Figure S3, and Figure S4). The Dazao-*stony* strain was backcrossed with Dazao for >24 generations, suggesting that at least 99.99% ($1 - (1/2)^{24}$) of the genetic composition is identical between Dazao and Dazao-*stony*. Theoretically, the expression patterns of *BmLcp18*, *BmLcp22*, and *BmLcp30* and content distribution of chitin should be similar in different cuticle positions between Dazao and Dazao-*stony*. However, the expression patterns of the four genes and chitin content in Dazao-*stony* internode and intersegmental fold are opposite to those in Dazao (Figure 6B), similar to the cases in Figure 5A-iv [AP *vs.* (PP + in-f), intersegmental fold (in-f)] and Figure S7A-iii and -vi. Therefore, we speculate that the phenotypic appearance of PP is converted to that of the intersegmental fold in *stony* mutant (Figure 1, B and C, Figure 6A-iii and -iv, Figure 6B, and Figure S7). This finding signifies that the greater part of intersegmental fold selected may be the posterior margin of the corresponding internode, resulting from dysfunctional BmorCPR2 (Figure S7C). In *stony* mutant, conversion from PP to the intersegmental fold reduces the circle area of the cuticle significantly, leading to lower ability of internodes to contain internal tissues and organs, and consequently, it has a tighter larval body. Simultaneously, the strong internal pressure extrapolates the abnormal intersegmental fold (enlarged) and generates bulges and, in turn, abnormal body shape in the *stony* mutant (Figure 1, A–C). Moreover, cuticle flexibility and larval athletic ability are impeded (Figure 1, F–J, and Figure S1, F–K). In *Manduca sexta* larvae, bulgy intersegmental membrane (via treatment with cyromazine) also leads to larval movement and cuticle flexibility impairment (Reynolds and Blakey 1989; Kotze and Reynolds 1990, 1991). Further research is warranted to determine the precise nature of interactions (localization and possible crosslinking) between BmorCPR2 and chitin in different parts of the segment at the ultrastructural level.

The model to explain the phenotype of the stony mutant

Based on the data obtained, we proposed a model to explain the phenotype of the *stony* mutant as follows: lack of normal *BmorCPR2* protein induces a reduction in the cuticle chitin content, which limits growth and extension of the cuticle. Meanwhile, disruption of the *BmorCPR2* gene causes the

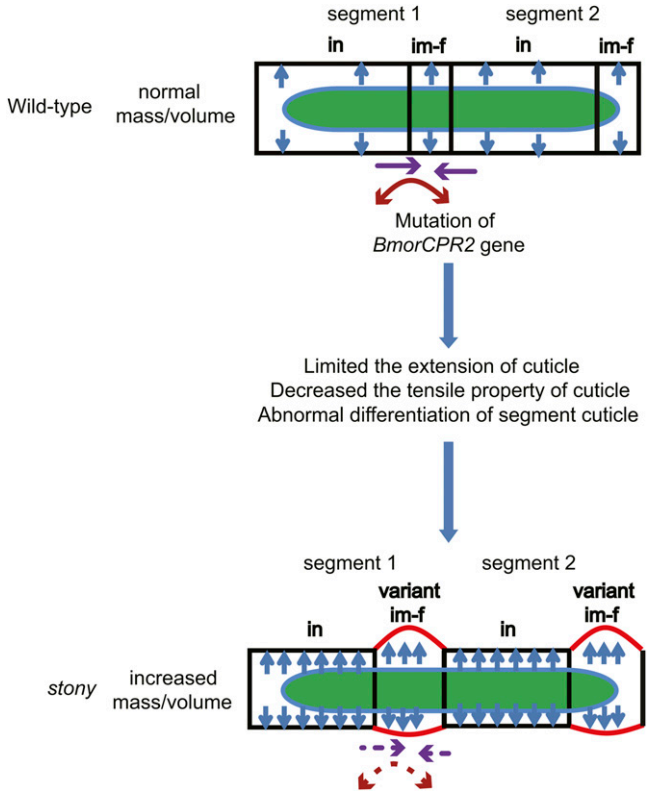

Figure 7 Schematic overview of the phenotype of *stony* mutant. Dysfunctional BmorCPR2 leads to cuticle extend blockage, decrease in tensile property, and abnormal differentiation of various parts in the segment cuticle, resulting in significant increase of the internal pressure of the body cavity and pushing out of the increscent and variant intersegmental fold. These factors lead to tightness and hardness, abnormal body shape, and marked decrease in adaptability of larvae. in, internode; im-f, intersegmental fold. The green region shows midgut content. Blue arrows indicate internal pressure of the body cavity, and the solid purple arrow represents telescopic movement between segments. The dotted purple arrow represents the deficiency of telescopic movement between segments. Red solid and dotted circular arrows represent normal crooking and deficiency of crooking capacity of the ventral side, respectively.

posterior part of the internode to switch to intersegmental fold in appearance, leading to reduced surrounding internode area and cuticle tensile property. Accumulation of these variations results in intense antagonism between the gradual increase in internal contents and growth-limited cuticle and consequently, an obvious increase in the internal pressure of larval body cavity, causing the larval body to become stiff, tight, and hard and reducing its ability to buffer shock. Simultaneously, due to strong pressure in the body cavity, the posterior of each segment is pushed outward, causing abnormal body-shape and athletic ability defects (Figure 7). In *Manduca sexta*, the levels and incorporation of glycine of cuticular protein in larvae treated with cyromazine are reduced (Kotze and Reynolds 1991), and the phenotype and physiological characteristics of treated larvae similar to those of the *stony* mutant (Reynolds and Blakey 1989; Kotze and Reynolds 1990) (Figure 1, Figure 4, Figure 5, and Figure S1, E–K). Accordingly, we speculate that the cyromazine target is associated with BmorCPR2 or candidate genes of other body-shape mutants with similar phenotypic and physiological characteristics to *stony* in silkworm. We aim to verify this hypothesis in subsequent analyses.

Conclusion

The number of chitin-binding cuticular proteins in different insect genomes varies significantly (Magkrioti *et al.* 2004; Weinstock *et al.* 2006; Karouzou *et al.* 2007; Cornman *et al.* 2008; Futahashi *et al.* 2008; Richards *et al.* 2008; Willis 2010; Gilbert 2011, Chap. 5). Even within the same insect, they are selectively switched on or off at different developmental stages as well as in cuticles with different physical properties. Therefore, the chitin-binding cuticular proteins involved in modeling and maintaining body shape differ in identity and function according to the insect and developmental stage (Soares *et al.* 2007; Okamoto *et al.* 2008; Togawa *et al.* 2008; Charles 2010), and our results show that mutation of the *BmorCPR2* gene alters the overall morphology of larvae, validating its role in body-shape determination in silkworm. These findings suggest that the number, expression patterns, and functional diversification of chitin-binding cuticular proteins represent key factors in understanding the diversity of insect body shape and provide a reference to analyze the molecular basis for other body-shape mutants in silkworm. In addition, BmorCPR2 homologs are abundant in *Lepidoptera* insects, including agricultural pests. Unlike domesticated silkworm, wild *Lepidoptera* larvae lack human protection, and their survival depends on normal differentiation, structure, and function of the cuticle. If wild *Lepidoptera* larvae appear to have a similar phenotype to *stony*, their adaptability will be seriously affected, with lethal consequences. Determination of the characteristics of BmorCPR2 may thus provide a reference for potential utilization of these cuticular protein types in pest control strategies for *Lepidoptera*.

Acknowledgments

We thank Professor Kunyan Zhu and professor Jianzhen Zhang for chitin extraction and quantification, Dr. Yuanhao Li and Dr. Songyuan Wu for valuable advice, and M. S. Kunpeng Lu for cuticle dissection. We are extremely grateful to Ms. Yanyan wang for her guidance on Dynamic Mechanical Analyzer analysis. This work was supported by National Basic Research 973 Program of China Grant (No. 2012CB114600), Hi-Tech Research and Development 863 Program of China Grant (2013AA102507), the National Natural Science Foundation of China (Nos. 31302038 and 31072088), Natural Science Foundation Project of ChongQing (CSTC) (No. cstc2013jcyjA0634), Fundamental Research Funds for the Central Universities in China (No. XDJK2013A001), and Par-Eu Scholars Program.

Literature Cited

Andersen, S. O., 2011 Are structural proteins in insect cuticles dominated by intrinsically disordered regions? Insect Biochem. Mol. Biol. 41: 620–627.

Andersen, S. O., P. Hojrup, and P. Roepstorff, 1995 Insect cuticular proteins. Insect Biochem. Mol. Biol. 25: 153–176.

Arakane, Y., J. Lomakin, S. H. Gehrke, Y. Hiromasa, J. M. Tomich *et al.*, 2012 Formation of rigid, non-flight forewings (elytra) of a beetle requires two major cuticular proteins. PLoS Genet. 8: e1002682.

Arakane, Y., 2013 Functional genomics of TcCPR4 belongs to RR-1 CP family in the red flourbeetle, Tribolium castaneum. Fourth International Conference of Insect Physiology, Biochemistry and Molecular Biology, Nanjing, China. Available at: http://www.meeting.edu.cn/meeting/webmedia/jingpin/ipmb2013/pic/abstract.pdf.

Bouligand, Y., 1965 On a twisted fibrillar arrangement common to several biologic structures. C. R. Acad. Sci. Hebd. Seances Acad. Sci. D 261: 4864–4867.

Brackenbury, J., 1997 Caterpillar kinematics. Nature 390: 453.

Carter, D., and M. Locke, 1993 Why caterpillars do not grow short and fat. Int. J. Insect Morphol. Embryol. 22: 81–102.

Chang, Y. F., J. S. Imam, and M. F. Wilkinson, 2007 The nonsense-mediated decay RNA surveillance pathway. Annu. Rev. Biochem. 76: 51–74.

Charles, J. P., 2010 The regulation of expression of insect cuticle protein genes. Insect Biochem. Mol. Biol. 40: 205–213.

Chaudhari, S. S., Y. Arakane, C. A. Specht, B. Moussian, D. L. Boyle *et al.*, 2011 Knickkopf protein protects and organizes chitin in the newly synthesized insect exoskeleton. Proc. Natl. Acad. Sci. USA 108: 17028–17033.

Chaudhari, S. S., Y. Arakane, C. A. Specht, B. Moussian, K. J. Kramer *et al.*, 2013 Retroactive maintains cuticle integrity by promoting the trafficking of Knickkopf into the procuticle of *Tribolium castaneum*. PLoS Genet. 9: e1003268.

Cornman, R. S., and J. H. Willis, 2009 Annotation and analysis of low-complexity protein families of *Anopheles gambiae* that are associated with cuticle. Insect Mol. Biol. 18: 607–622.

Cornman, R. S., T. Togawa, W. A. Dunn, N. He, A. C. Emmons *et al.*, 2008 Annotation and analysis of a large cuticular protein family with the R&R Consensus in *Anopheles gambiae*. BMC Genomics 9: 22.

Dai, F. Y., L. Qiao, X. L. Tong, C. Cao, P. Chen *et al.*, 2010 Mutations of an arylalkylamine-*N*-acetyltransferase, Bm-iAANAT, are responsible for silkworm melanism mutant. J. Biol. Chem. 285: 19553–19560.

Delon, I., and F. Payre, 2004 Evolution of larval morphology in flies: get in shape with shavenbaby. Trends Genet. 20: 305–313.

Feschotte, C., 2008 Transposable elements and the evolution of regulatory networks. Nat. Rev. Genet. 9: 397–405.

Futahashi, R., S. Okamoto, H. Kawasaki, Y. S. Zhong, M. Iwanaga *et al.*, 2008 Genome-wide identification of cuticular protein genes in the silkworm, *Bombyx mori*. Insect Biochem. Mol. Biol. 38: 1138–1146.

Gilbert, L. I., 2011 *Insect Molecular Biology and Biochemistry*. Academic Press, New York.

Guan, X., B. W. Middlebrooks, S. Alexander, and S. A. Wasserman, 2006 Mutation of TweedleD, a member of an unconventional cuticle protein family, alters body shape in Drosophila. Proc. Natl. Acad. Sci. USA 103: 16794–16799.

Jasrapuria, S., Y. Arakane, G. Osman, K. J. Kramer, R. W. Beeman *et al.*, 2010 Genes encoding proteins with peritrophin A-type chitin-binding domains in *Tribolium castaneum* are grouped into three distinct families based on phylogeny, expression and function. Insect Biochem. Mol. Biol. 40: 214–227.

Jasrapuria, S., C. A. Specht, K. J. Kramer, R. W. Beeman, and S. Muthukrishnan, 2012 Gene families of cuticular proteins analogous to peritrophins (CPAPs) in *Tribolium castaneum* have diverse functions. PLoS ONE 7: e49844.

Karouzou, M. V., Y. Spyropoulos, V. A. Iconomidou, R. S. Cornman, S. J. Hamodrakas *et al.*, 2007 Drosophila cuticular proteins with the R&R Consensus: annotation and classification with a new tool for discriminating RR-1 and RR-2 sequences. Insect Biochem. Mol. Biol. 37: 754–760.

Kiguchi, K., 1981 Ecdysteroid levels and developmental events during larval moulting in the silkworm, *Bombyx mori*. J. Insect Physiol. 27: 805–812.

Kotze, A. C., and S. E. Reynolds, 1990 Mechanical properties of the cuticle of *Manduca sexta* larvae treated with cyromazine. Pestic. Biochem. Physiol. 38: 267–272.

Kotze, A. C., and S. E. Reynolds, 1991 An examination of cuticle chitin and protein in cyromazine-affected *Manduca sexta* larvae. Pestic. Biochem. Physiol. 41: 14–20.

Lease, H. M., and B. O. Wolf, 2010 Exoskeletal chitin scales isometrically with body size in terrestrial insects. J. Morphol. 271: 759–768.

Lin, H. T., A. L. Dorfmann, and B. A. Trimmer, 2009 Soft-cuticle biomechanics: a constitutive model of anisotropy for caterpillar integument. J. Theor. Biol. 256: 447–457.

Locke, M., 1970 The molt/intermolt cycle in the epidermis and other tissues of an insect *Calpodes ethlius* (Lepidoptera, Hesperiidae). Tissue Cell 2: 197–223.

Magkrioti, C. K., I. C. Spyropoulos, V. A. Iconomidou, J. H. Willis, and S. J. Hamodrakas, 2004 cuticleDB: a relational database of arthropod cuticular proteins. BMC Bioinformatics 5: 138.

Merzendorfer, H., and L. Zimoch, 2003 Chitin metabolism in insects: structure, function and regulation of chitin synthases and chitinases. J. Exp. Biol. 206: 4393–4412.

Mizoguchi, A., Y. Ohashi, K. Hosoda, J. Ishibashi, and H. Kataoka, 2001 Developmental profile of the changes in the prothoracicotropic hormone titer in hemolymph of the silkworm *Bombyx mori*: correlation with ecdysteroid secretion. Insect Biochem. Mol. Biol. 31: 349–358.

Moussian, B., 2010 Recent advances in understanding mechanisms of insect cuticle differentiation. Insect Biochem. Mol. Biol. 40: 363–375.

Moussian, B., H. Schwarz, S. Bartoszewski, and C. Nusslein-Volhard, 2005 Involvement of chitin in exoskeleton morphogenesis in *Drosophila melanogaster*. J. Morphol. 264: 117–130.

Moussian, B., E. Tang, A. Tonning, S. Helms, H. Schwarz *et al.*, 2006 Drosophila Knickkopf and Retroactive are needed for epithelial tube growth and cuticle differentiation through their specific requirement for chitin filament organization. Development 133: 163–171.

Nakato, H., M. Takekoshi, T. Togawa, S. Izumi, and S. Tomino, 1997 Purification and cDNA cloning of evolutionally conserved larval cuticle proteins of the silkworm, *Bombyx mori*. Insect Biochem. Mol. Biol. 27: 701–709.

Neville, A. C., 1975 *Biology of the Arthropod Cuticle*. Springer-Verlag, New York.

Neville, A. C., and B. M. Luke, 1969 A two-system model for chitin-protein complexes in insect cuticles. Tissue Cell 1: 689–707.

Okamoto, S., R. Futahashi, T. Kojima, K. Mita, and H. Fujiwara, 2008 Catalogue of epidermal genes: genes expressed in the epidermis during larval molt of the silkworm *Bombyx mori*. BMC Genomics 9: 396.

Papandreou, N. C., V. A. Iconomidou, J. H. Willis, and S. J. Hamodrakas, 2010 A possible structural model of members of the CPF family of cuticular proteins implicating binding to components other than chitin. J. Insect Physiol. 56: 1420–1426.

Rebers, J. E., and L. M. Riddiford, 1988 Structure and expression of a *Manduca sexta* larval cuticle gene homologous to Drosophila cuticle genes. J. Mol. Biol. 203: 411–423.

Rebers, J. E., and J. H. Willis, 2001 A conserved domain in arthropod cuticular proteins binds chitin. Insect Biochem. Mol. Biol. 31: 1083–1093.

Reynolds, S. E., and J. K. Blakey, 1989 Cyromazine causes decreased cuticle extensibility in larvae of the tobacco hornworm, *Manduca sexta*. Pestic. Biochem. Physiol. 35: 251–258.

Richards, O. W., and R. G. Davies, 1977 *IMMS' General Textbook of Entomology*. Halsted Press, New York.

Richards, S., R. A. Gibbs, G. M. Weinstock, S. J. Brown, R. Denell *et al.*, 2008 The genome of the model beetle and pest *Tribolium castaneum*. Nature 452: 949–955.

Soares, M. P., M. Elias-Neto, Z. L. Simoes, and M. M. Bitondi, 2007 A cuticle protein gene in the honeybee: expression during development and in relation to the ecdysteroid titer. Insect Biochem. Mol. Biol. 37: 1272–1282.

Tang, L., J. Liang, Z. Zhan, Z. Xiang, and N. He, 2010 Identification of the chitin-binding proteins from the larval proteins of silkworm, *Bombyx mori*. Insect Biochem. Mol. Biol. 40: 228–234.

Togawa, T., H. Nakato, and S. Izumi, 2004 Analysis of the chitin recognition mechanism of cuticle proteins from the soft cuticle of the silkworm, *Bombyx mori*. Insect Biochem. Mol. Biol. 34: 1059–1067.

Togawa, T., W. A. Dunn, A. C. Emmons, J. Nagao, and J. H. Willis, 2008 Developmental expression patterns of cuticular protein genes with the R&R Consensus from *Anopheles gambiae*. Insect Biochem. Mol. Biol. 38: 508–519.

Weinstock, G. M., G. E. Robinson, R. A. Gibbs, G. M. Weinstock, K. C. Worley *et al.*, 2006 Insights into social insects from the genome of the honeybee *Apis mellifera*. Nature 443: 931–949.

Wigglesworth, V. B., 1957 The physiology of insect cuticle. Annu. Rev. Entomol. 2: 37–54.

Willis, J. H., 2010 Structural cuticular proteins from arthropods: annotation, nomenclature, and sequence characteristics in the genomics era. Insect Biochem. Mol. Biol. 40: 189–204.

Willis, J. H., V. A. Iconomidou, R. F. Smith, and S. J. Hamodrakas, 2005 Cuticular proteins, pp. 79–110 in *Comprehensive Molecular Insect Science*, Vol. 4, edited by L. I. Gilbert, K. Iatrou, and S. S. Gill. Elsevier, Oxford, UK.

Yamamoto, K., J. Nohata, K. Kadono-Okuda, J. Narukawa, M. Sasanuma *et al.*, 2008 A BAC-based integrated linkage map of the silkworm *Bombyx mori*. Genome Biol. 9: R21.

Zhang, J., and K. Y. Zhu, 2006 Characterization of a chitin synthase cDNA and its increased mRNA level associated with decreased chitin synthesis in *Anopheles quadrimaculatus* exposed to diflubenzuron. Insect Biochem. Mol. Biol. 36: 712–725.

Communicating editor: B. Sullivan

GENETICS

Supporting Information
http://www.genetics.org/lookup/suppl/doi:10.1534/genetics.113.158766/-/DC1

Mutation of a Cuticular Protein, *BmorCPR2*, Alters Larval Body Shape and Adaptability in Silkworm, *Bombyx mori*

Liang Qiao, Gao Xiong, Ri-xin Wang, Song-zhen He, Jie Chen, Xiao-ling Tong, Hai Hu, Chun-lin Li, Ting-ting Gai, Ya-qun Xin, Xiao-fan Liu, Bin Chen, Zhong-huai Xiang, Cheng Lu, and Fang-yin Dai

DOI: 10.1534/genetics.113.158766

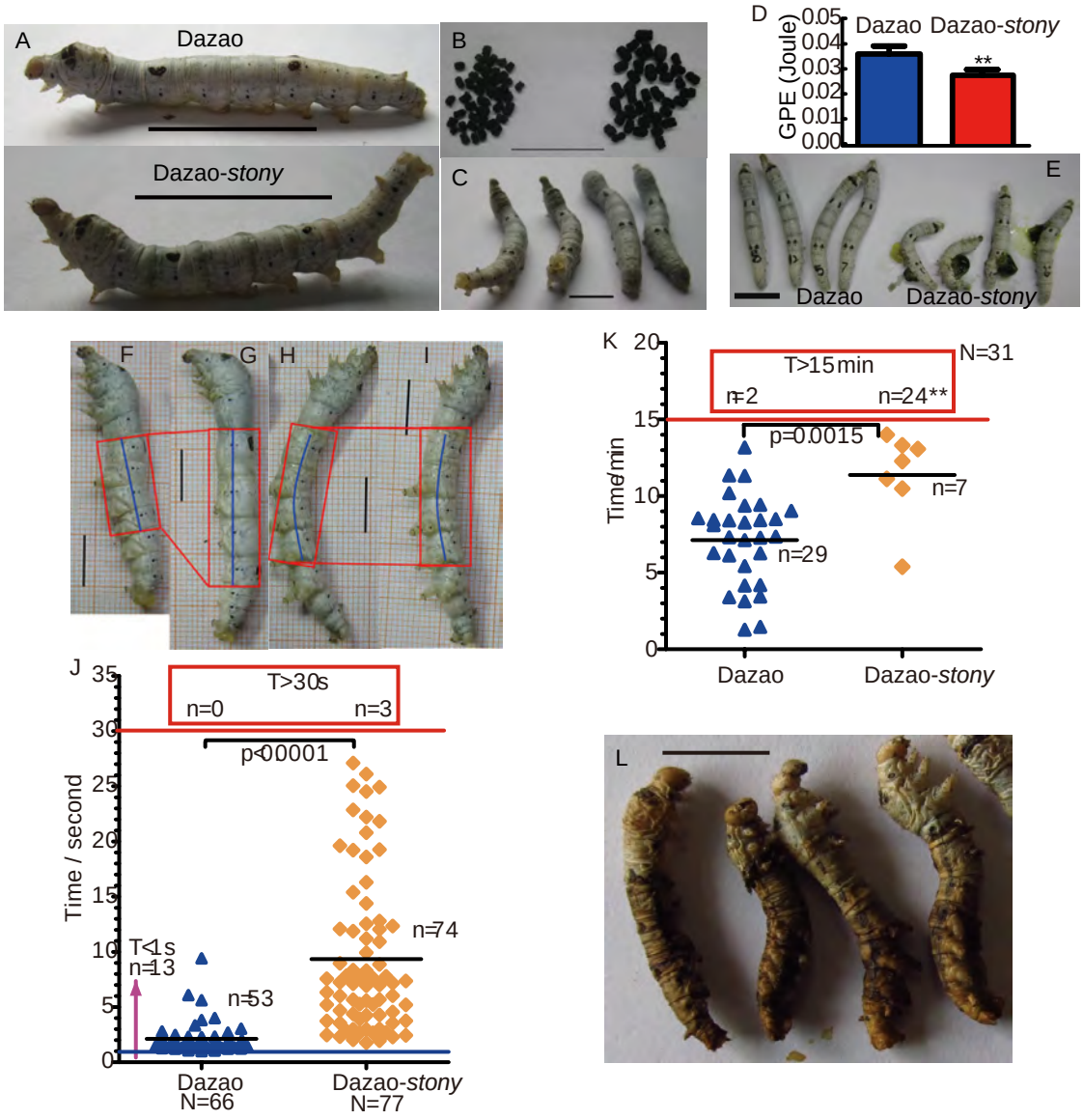

Figure S1 Additional phenotype and behavior assays of *stony* mutant. A. represents the phenotypes of the sides of Dazao and Dazao-*stony*, respectively. Scale bar: 2cm. B. Phenotypes of the excrement of Dazao and Dazao-*stony*. Scale bar: 2 cm. C. Rectocele phenomenon of Dazao-*stony*. Scale bar: 1 cm. D. Average of the GPE (gravitational potential energy) of Dazao and Dazao-*stony* strains selected for the dropping experiment, h=2m, (n=20). Data represent mean values ± S.D. Student's t test, ** $p<0.01$. E. Body rupture of Dazao-*stony* in the dropping experiment. Scale bar: 1 cm. F and H represent the phenotypes of Dazao and Dazao-*stony* injected with air, respectively. Scale bar: 1 cm. G and I represent the phenotypes of stretched individuals in F and H , respectively. Scale bar: 1 cm. The red box includes the abdomen segments (2^{nd} to 5^{th}) and the blue line represents length. J. Comparative inversion tests on Dazao and Dazao-*stony*. Both red and blue lines represent threshold time. The numbers in the red box indicate individuals which cannot turn over in 30 s The time of turning over in Dazao was significantly lower than that in Dazao-*stony* within the set time-frame (30 s). Mann-Whitney *U*-test. $P<0.0001$. K. crawling ability test under food inducement. The red line represents the threshold time. The numbers in the red box indicate individuals which cannot touch mulberry leaves in 15 min. ** represents $p<0.01$ χ^2-test. Compared to Dazao, Dazao-*stony* needed more time to touch mulberry leaves within the set time-frame (15 min). Mann-Whitney *U*-test. $P<0.0001$. Additionally, due to strong pressure in the body cavity, physical coordination of Dazao-*stony* was significantly poorer than that of Dazao during the crawling process (File S8). L. Phenotypes of *stony* mutants at the beginning of 5^{th} instar with molting difficulties. Scale bar: 1 cm.

Full-length cDNA of *BmorCPR3*

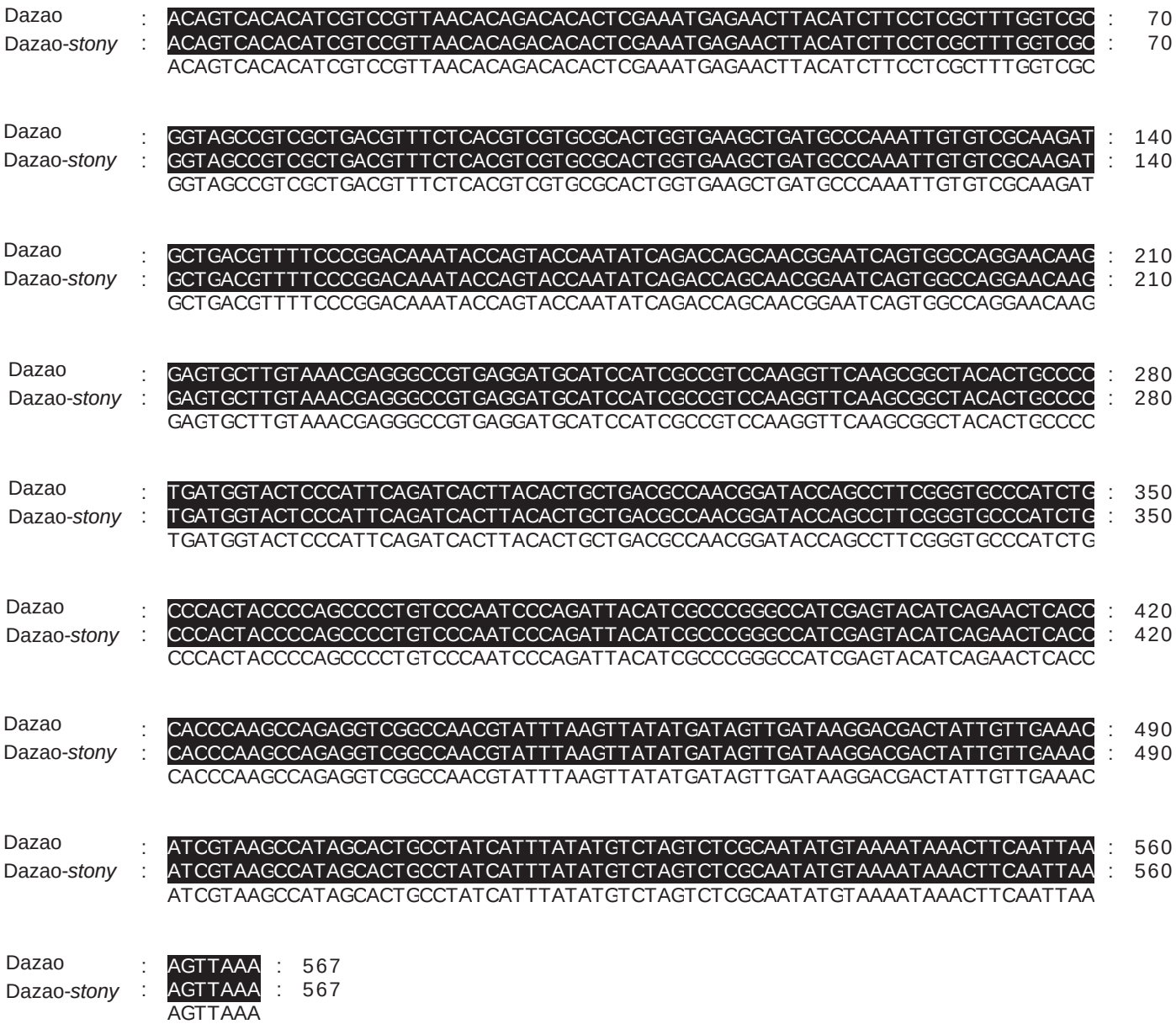

Figure S2 Full-length *BmorCPR3* cDNA sequences of Dazao and Dazao-*stony*.

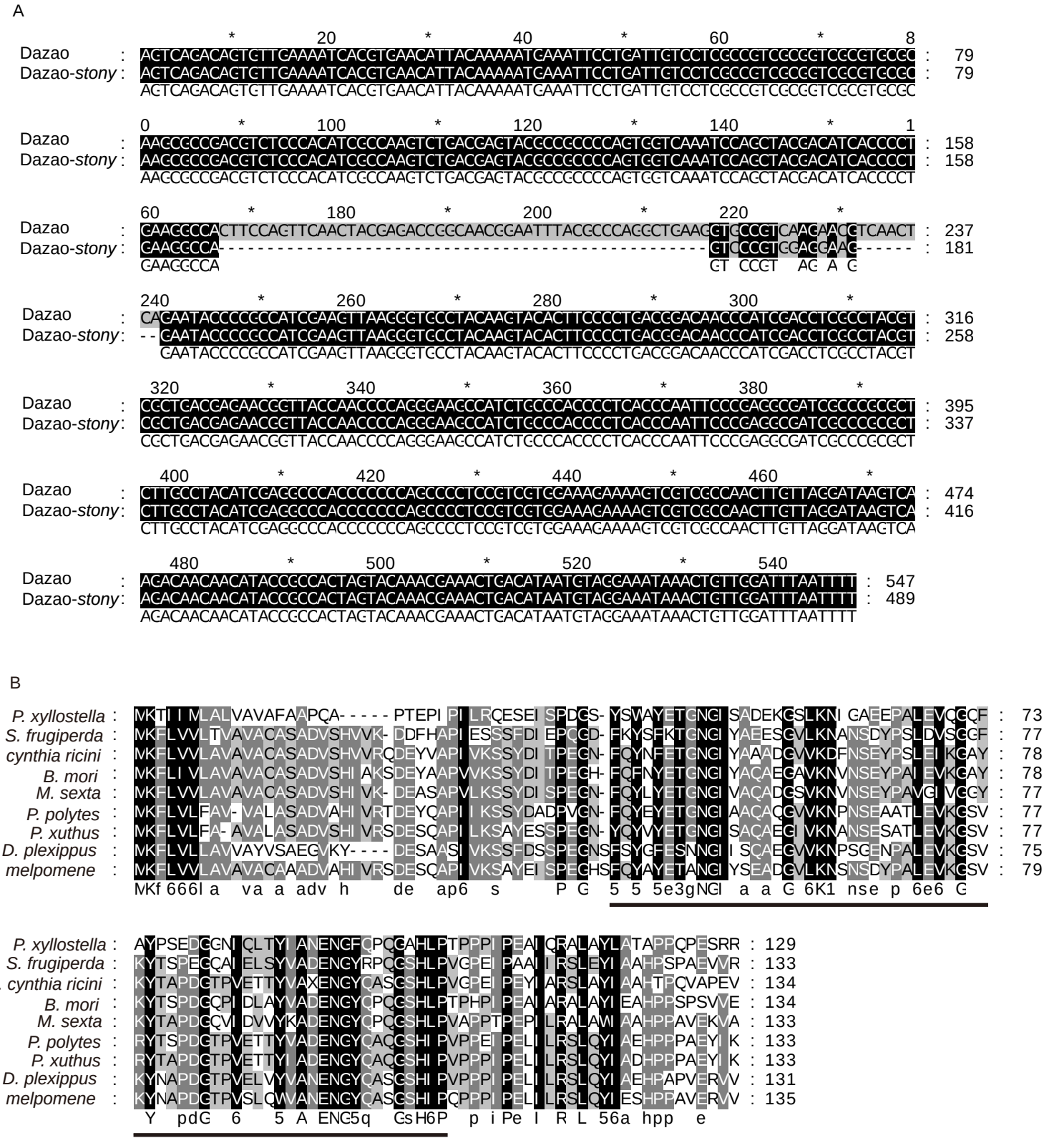

Figure S3 Sequence characteristics of *BmorCPR2* between Dazao and Dazao-*stony*. A. Full-length cDNA sequences of *BmorCPR2* between Dazao and Dazao-*stony*. B. Alignment of BmorCPR2 and orthologs among nine Lepidopera species. The orthologs were identified using BLAST (blastp and tblastn), known genomes or EST databases of selected Lepidopera insects, NCBI, CuticleDB (http://bioinformatics.biol.uoa.gr/cuticleDB and OrhtoDB (http://cegg.unige.ch/orthodb6). Sequence alignment using Muscle program (http://www.ebi.ac.uk/Tools/msa/muscle/), is listed as follows: *Bombyx mori* BmorCPR2, *Papilio polytes* CPR2, BAM18876.1, *Papilio xuthus* CPR2, BAG30800.1, *Danaus plexippus* EHJ77392.1, *Manduca sexta* Msex000162-RB, (Manduca base), *Heliconius melpomene* HMEL002550-PA, (Heliconius Genome Project), *Samia cynthia ricini* I10A02NGRL0007_H08 (SilkBase), *Plutella xylostella* Px003256.1 (Diamondback moth Genome Database), *Spodoptera frugiperda* Sf1P23819-5-1, (SPODOBASE). The black line represents the RR1 motif.

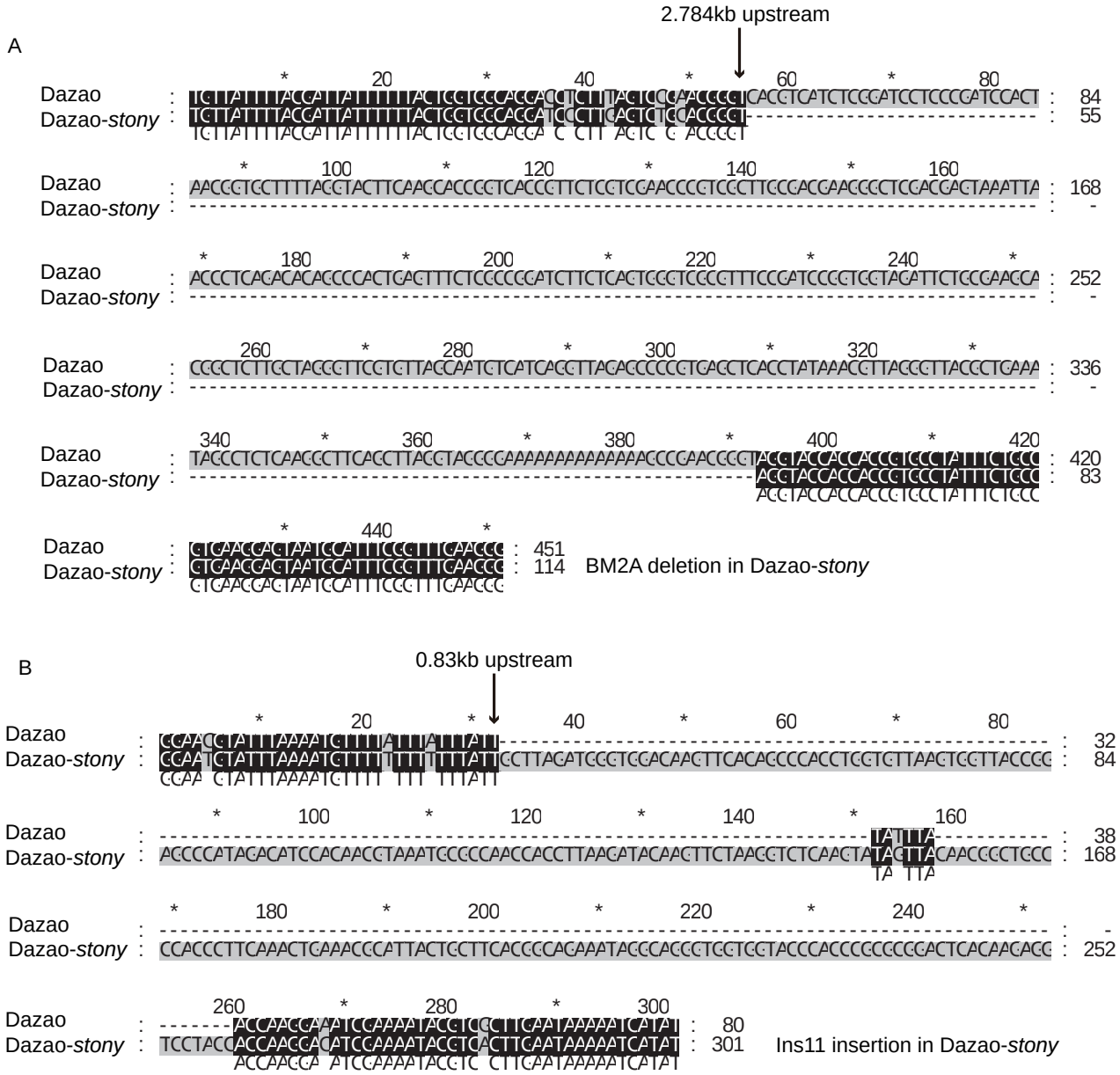

Figure S4 Comparison of the ~2.78 kb (A) and ~0.83 kb (B) upstream genomic sequences of *BmorCPR2* of Dazao and Dazao-*stony*.

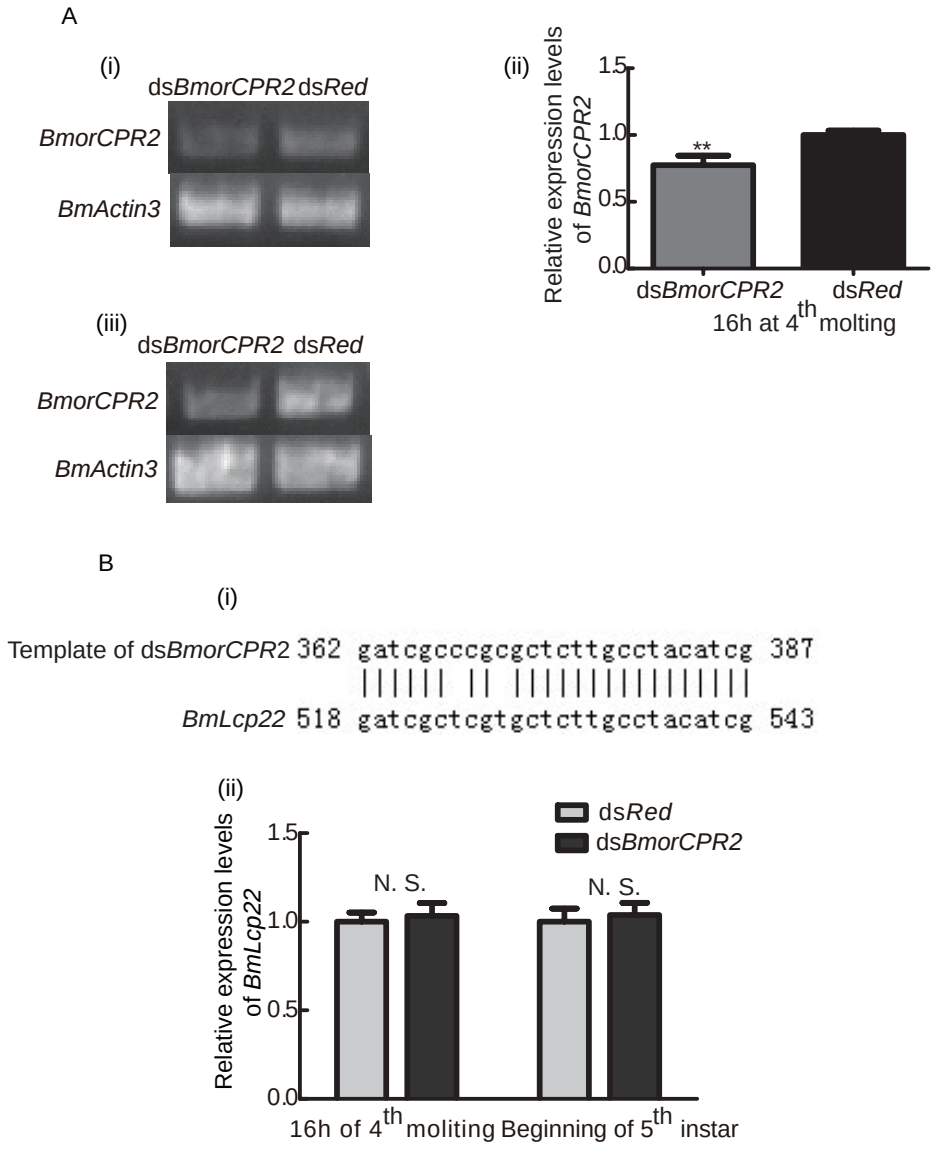

Figure S5 Analysis of the effects of RNAi. A. RT-PCR and qRT-PCR analysis. (i) and (ii) represent expression of *BmorCPR2* in larvae subjected to RNAi at 16 h of 4th molting. (iii) represent expression of *BmorCPR2* in larvae subjected to RNAi at beginning of 5th instar. B. Detection of RNAi off-target effects. (i) Nucleic acid alignment between *BmLcp22* and ds*BmorCPR2* template. (ii) Relative expression levels of *BmLcp22*. Data are presented as mean values ± S.D. N.S. indicates no significant differences in the *BmLcp22* expression levels between ds*BmorCPR2* and ds*Red* groups.

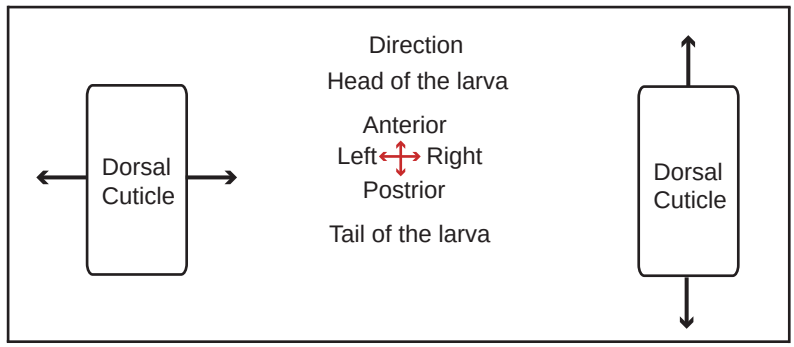

Figure S6 Schematic diagram of manipulation in the stretching test. Black arrowhead represents the stretching direction and red cross arrowhead indicates location.

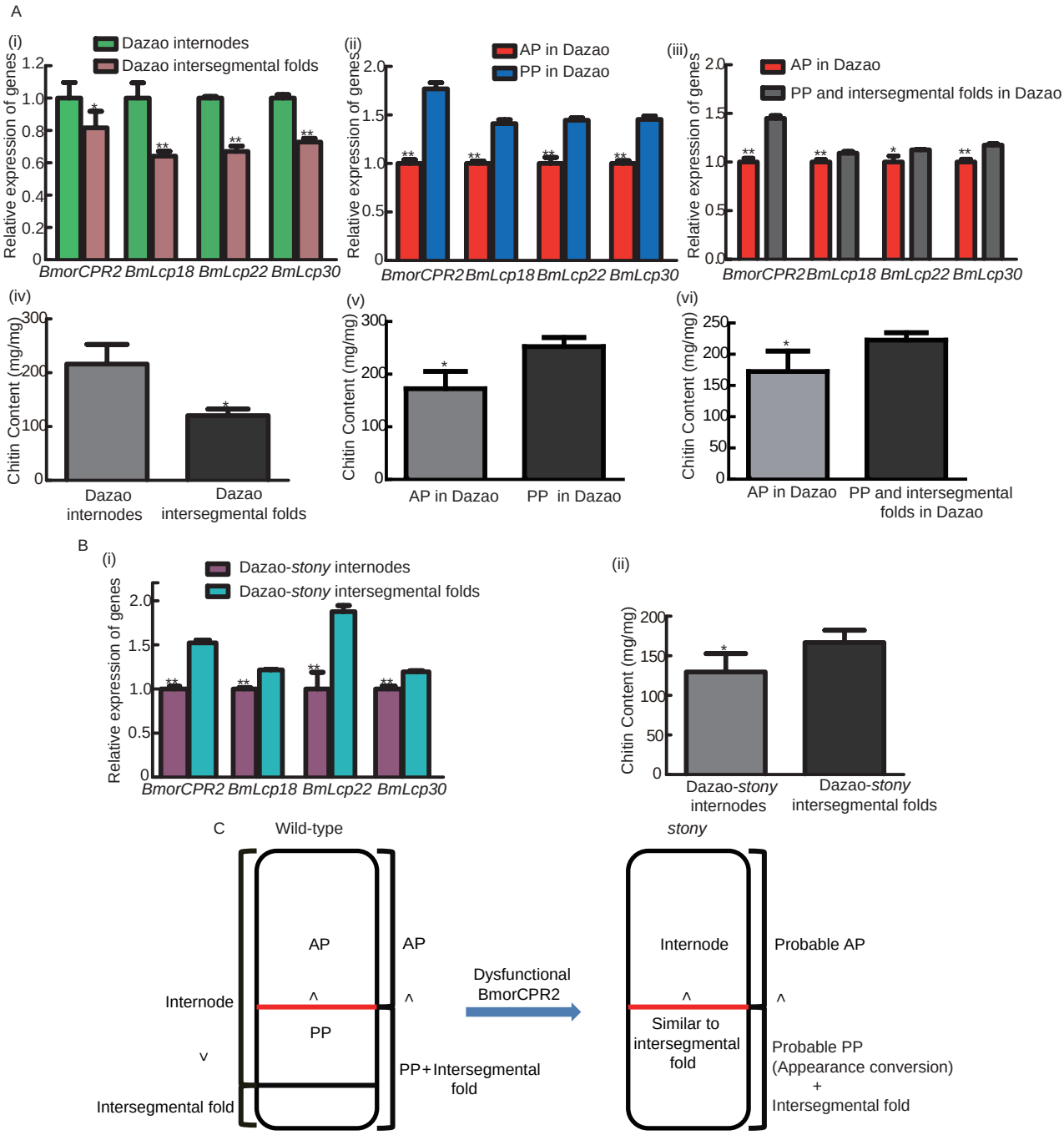

Figure S7 Detailed data of Gene expression profiles and chitin distribution in various parts of segmental cuticle in Dazao and Dazao-*stony*. A. Detailed data of cuticular gene expression profiles and chitin distribution in different parts of Dazao dorsal segment cuticle. (i) and (iv) represent gene expression profiles (n=3) and chitin content (n=4) of the internodes and intersegmental folds in Dazao, respectively. (ii) and (v) represent the gene expression profiles (n=3) and chitin content (n=3) of AP and PP in Dazao, respectively. (iii) and (vi) represent gene expression profiles (n=3) and chitin content (n=3) of the anterior and remaining parts (posterior parts and intersegmental folds) in Dazao, respectively. Data are presented as mean values ± S.D. Student's *t*-test, *represent $p<0.05$, **represents $p<0.01$. B. Detailed data of cuticular gene expression profiles and chitin quantification in different parts of Dazao-*stony* segment. (i) represents gene expression profiles (n=3) of internodes and intersegmental folds in Dazao-*stony*. Data are presented as mean values ± S.D. Student's *t*-test, ** represents $p<0.01$. (ii) represents the chitin content (n=4) of the internodes and variant intersegmental folds in Dazao-*stony*. Data are presented as mean values ± S.D. Student's *t*-test, *represents $p<0.05$. C. Derived schematic diagram for formation of the abnormal intersegmental fold in *stony* mutant. The black line represents the boundary of internode and intersegmental fold in Dazao. The red line represent the boundary of AP and PP. The tip of symbol '∧' and symbol '∨' point to the parts with lower genes expression and chitin content.

File S1

Supporting Methods

(a) Detailed operation of physiology test and behavior assays

In the dropping experiment, 20 Dazao-*stony* and Dazao individuals were subjected to a height of 2 m, followed by motion of a free falling body. The numbers of ruptured Dazao and Dazao-*stony* individuals were added up to compare their abilities to buffer the shock. To compare the flexibility and nesting ability of internode and intersegmental fold between Dazao and Dazao-*stony*, we injected 4 mL air into larvae, and stretch along the anterior-posterior axis of the body. To determine abdomen crooking ability, larvae were inverted to turn the dorsum down and the thorax pressed lightly to prevent writhing to the two sides. Subsequently, inversion towards the abdomen was observed. The number of individuals able to writhe to abdomen, time needed, and the angle between the dorsum and horizontal plane (performed using the digital camera, image J, and angle test software) were recorded. To determine grasping state and duration, larvae were placed on the middle of the mallet (diameter: ~0.9 and ~1.4 cm) in the larval grasping experiment. In the inversion assay analyzing dorsum crooking ability, we fixed the back of larvae on the plane carefully and unclamped them quickly to record the rolling state and time required. We additionally performed a food-inducing crawling experiment. Specifically, 5th instar day 5 larvae subjected to 10 h starvation were selected. Larvae were placed ~4 cm away from fresh mulberry leaves(Dethier 1941; Slifer 1955), and their crawling behavior and time to reach leaves recorded. In the phenotype analysis, physiology test and behavior assays, healthy Dazao and Dazao-*stony* larvae on day 5 of 5th instar glutted with mulberry leaf and subsequently starved for 4 h were selected, except for those used in the crawling experiment.

(b) Detailed operation of chitin binding

The soluble proteins extracted from sediment were dialyzed to eliminate SDS using Tang's method (TANG *et al.* 2010). Ethanol in mixed chitin beads was discarded and chitin resuspended with binding buffer (20 mM HEPES, 15 mM NaCl, pH 7.4). Next, ~100 μg cuticular protein of Dazao was mixed with chitin (volume ratio of 1:2, total volume 1 ml) in a 1.5 mL EP tube. The solution was incubated at 16°C for 4 h and shaken at 40 rpm. Following centrifugation (9000g, 4°C), the supernatant (S-incubation) was collected and added to 1.2 mL washing buffer (20 mM HEPES, 1 M NaCl, pH 7.4). Next, the mixture was shaken for 40 s and centrifuged under set conditions (9000g, 4°C). The supernatant was removed and the wash step repeated once. The final supernatant fraction (W2) and remaining chitin sediment were collected. S-incubation, W2 and chitin sediment were mixed with Laemmli sample buffer and heated at 95°C for 10 min, and the supernatant collected and analyzed using 15% SDS-PAGE.

(c) Detailed operation of LC-MS/MS

The gel was suspended in 200-400 μL decolorizing agent (30% ACN/100 mM NH4HCO3) until transparent, the supernatant was removed and frozen to dryness. Next, 100 mM DTT was added and incubated for 30 min under 56°C. After removal of the supernatant, 200 mM IAA was added, and the sample incubated in the dark for 20 min. The supernatant was removed and the sample treated with 100 mM NH4HCO3 at room temperature for 15 min. Following removal of the supernatant, ACN was added. After 5 min, the supernatant was blotted and frozen to dryness. Next, the dried sample was incubated overnight with 2.5-10 ng/μL Trypsin solution (37°C, about 20 h) and the enzymatic hydrolysate added to a new EP tube. We further added 100 μL extraction buffer（60%ACN/0.1%TFA）to the gel, followed by ultrasound for 15 min, combined with the enzymatic hydrolysate for freezing to dryness. The capillary performance liquid chromatography method was performed as follows: the chromatographic column was equilibrated with 95% solution A (0.1% formic acid), and the sample

loaded onto Trap column through an automatic sampler. Solution B (84% acetonitrile) flowthrough was as follows: 0-30 min with a linear gradient of 4 to 50%, 30-34 min with a linear gradient of 50 to 100%, and 34-40 min whereby the solution was maintained at 100%. The mass-charge ratios of peptide and peptide fragments were collected using the method for collecting MS2 scans after each full scan. Using BIOWORKS and SEQUEST programs, the raw file was searched in the related database (NCBI, http://silkworm.swu.edu.cn/silkdb/doc/download.html). Search steps were referenced to the procedure of Tang et al. (TANG *et al.* 2010).

Literature cited

DETHIER, V. G., 1941 The Function of the Antennal Receptors in Lepidopterous Larvae. Biological Bulletin **80:** 403-414.

SLIFER, E. H., 1955 The detection of odors and water vapor by grasshoppers (Orthoptera, Acrididae) and some new evidence concerning the sense organs which may be involved. Journal of Experimental Zoology **130:** 301-317.

TANG, L., J. LIANG, Z. ZHAN, Z. XIANG and N. HE, 2010 Identification of the chitin-binding proteins from the larval proteins of silkworm, Bombyx mori. Insect Biochem Mol Biol **40:** 228-234.

Files S2-S8

Available for download as AVI files at

http://www.genetics.org/lookup/suppl/doi:10.1534/genetics.113.158766/-/DC1

File S2 Video of dropping experiment

File S3 Video of abdominal crooking test

File S4 Video of grasping test on the large diameter mallets

File S5 Video of grasping test on the small diameter mallets

File S6 Video of inversion test with non hand-touch

File S7 Video of inversion test with hand-touch

File S8 Video of crawling ability test

Table S1 Primers used in this study

Available for download as an Excel file at http://www.genetics.org/lookup/suppl/doi:10.1534/genetics.113.158766/-/DC1

Table S2 LC-MS/MS identification in analysis of BmorCPR2 in target gels

Gel at ~15.3 kD	Protein requiring to be focused on	MW Charge	PI Rank	No. of unique peptids	UniquePepCount MH+	Sequence Coverage (%)	Peptide sequences	motif
Dazao-SDS PAGE	BmorCPR2	15270.2	5.06	5	1363.498	51.7	K.NVNSEYPAIEVK.G	RR-1
					1079.1851		K.SDEYAAPVVK.S	
					3295.4731		K.SSYDITPEGHFQFNYETGNGIYAQAEGAVK.N	
					1837.0688		R.ALAYIEAHPPSPSVVER.K	
					1965.2418		R.ALAYIEAHPPSPSVVERK.V	
Dazao-chitin binding	BmorCPR2	15270.2	5.06	3	1363.498	31.5	K.NVNSEYPAIEVK.G	RR-1
					1079.1851		K.SDEYAAPVVK.S	
					1837.0688		R.ALAYIEAHPPSPSVVER.K	
Dazao-*stony*-SDS PAGE	BmorCPR2	-[a]	-	-	-	-	-	-

[a] **undetected by LC-MS/MS**

Table S3 Statistic of RNAi

Treatment	Injected No.	No. of successful ecdysis	living and exhibiting RNAi phenotype	No. of Death during the molting stage
dsBmorCPR2	55	30	22	3
dsRed	43	41	0	2

Table S4 Amino acid identity of BmorCPR2 with its orthologs.

	B. mori	*P. polytes*	*P. xuthus*	*D. plexippus*	*M. sexta*	*H. melpomene*	*S. cynthia ricini*	*P. xyllostella*	*S. frugiperda*
B. mori	100%	59%	58%	57%	65%	55%	59%	54%	52%
P. polytes		100%	75%	58%	54%	58%	64%	40%	50%
P. xuthus			100%	60%	57%	64%	62%	47%	45%
D. plexippus				100%	51%	66%	58%	40%	46%
M. sexta					100%	58%	64%	50%	53%
H. melpomene						100%	54%	43%	44%
S. cynthia ricini							100%	45%	61%
P. xyllostella								100%	47%
S. frugiperda									100%